

This is an Open Access document downloaded from ORCA, Cardiff University's institutional repository:<https://orca.cardiff.ac.uk/id/eprint/102199/>

This is the author's version of a work that was submitted to / accepted for publication.

Citation for final published version:

Yang, Gaoxue, Li, Yongjun, Kerr, Andrew and Tong, Lili 2018. Accreted seamounts in North Tianshan, NW China: implications for the evolution of the Central Asian Orogenic Belt. *Journal of Asian Earth Sciences* 153 , pp. 223-237. 10.1016/j.jseaes.2017.05.010

Publishers page: <http://dx.doi.org/10.1016/j.jseaes.2017.05.010>

Please note:

Changes made as a result of publishing processes such as copy-editing, formatting and page numbers may not be reflected in this version. For the definitive version of this publication, please refer to the published source. You are advised to consult the publisher's version if you wish to cite this paper.

This version is being made available in accordance with publisher policies. See <http://orca.cf.ac.uk/policies.html> for usage policies. Copyright and moral rights for publications made available in ORCA are retained by the copyright holders.



# Accreted seamounts in North Tianshan, NW China: Implications for the evolution of the Central Asian Orogenic Belt

Gaoxue Yang<sup>a</sup>, Yongjun Li<sup>a</sup>, Andrew C. Kerr<sup>b</sup>, Lili Tong<sup>a</sup>

<sup>a</sup> The School of Earth Science and Resources, Chang'an University, Xi'an 710054, China

<sup>b</sup> School of Earth and Ocean Sciences, Cardiff University, Main Building, Park Place, Cardiff CF10 3AT, UK

## ABSTRACT

The Carboniferous Bayingou ophiolitic *mélange* is exposed in the North Tianshan accretionary complex in the southwestern part of the Central Asian Orogenic Belt (CAOB). The *mélange* is mainly composed of serpentinised ultramafic rocks (including harzburgite, lherzolite, pyroxenite, dunite and peridotite), pillowed and massive basalts, layered gabbros, radiolarian cherts, pelagic limestones, breccias and tuffs, and displays block-in-matrix structures. The blocks of ultramafic rocks, gabbros, basalts, cherts, and limestones are set in a matrix of serpentinised ultramafic rocks, massive basalts and tuffs. The basaltic rocks in the *mélange* show significant geochemical heterogeneity, and two compositional groups, one ocean island basalt-like, and the other mid-ocean ridge-like, can be distinguished on the basis of their isotopic compositions and immobile trace element contents (such as light rare earth element enrichment in the former, but depletion in the latter). The more-enriched basaltic rocks are interpreted as remnants/fragments of seamounts, derived from a deep mantle reservoir with low degrees (2–3%) of garnet lherzolite mantle melting. The depleted basalts most likely formed by melting of a shallower spinel lherzolite mantle source with ~15% partial melting. It is probable that both groups owe their origin to melting of a mixture between plume and depleted MORB mantle. The results from this study, when integrated with previous work, indicate that the Junggar Ocean crust (comprising a significant number of seamounts) was likely to have been subducted southward beneath the Yili-Central Tianshan block in the Late Devonian-Early Carboniferous. The seamounts were scraped-off and accreted along with the oceanic crust in an accretionary wedge to form the Bayingou ophiolitic *mélange*. We present a model for the tectonomagmatic evolution of this portion of the CAOB involving prolonged intra-oceanic subduction with seamount accretion

## 1. Introduction

Seamounts are one of the most ubiquitous landforms on Earth and at the present-day are distributed on all major oceanic plates (Wessel et al., 2010). Indeed, it has been reported that about 12,000 seamounts larger than 1.5 km in height can be found on the floor of the current oceans (Watts et al., 2010). Although seamounts can help us to better understand various deep Earth processes (e.g., Koppers and Watts, 2010), they are one of the least well-understood types of magmatic province and significant questions relating to their origin and structure remain (Foulger and Natland, 2003; Staudigel and Clague, 2010). Seamounts are generally interpreted to have formed by upwelling and decompression melting of mantle plumes (Morgan, 1971; Regelous et al., 2003) and thus can be recorders of both the speed and direction of plate motions (Tarduno et al., 2003). However, some seamounts form along lithospheric faults in response to plate flexure both during subduction (Hirano et al., 2006) and well away from plate boundaries (Machida et al., 2015).

Regardless of how they are formed seamounts migrate with the ocean plates and eventually reach active convergent margins (von Huene, 2008; Staudigel et al., 2010). However, because they represent areas of thicker-than-normal oceanic crust, they often accrete on the margin of subduction zones (Hoernle et al., 2002; Buchs et al., 2011). The attempted subduction of seamounts has also been linked to earthquake generation (Kodaira et al., 2000; Singh et al., 2011), submarine landslides (Ruh, 2016), as well as crustal erosion at subduction zones (Ranero and van Huene, 2000). The accretion of seamounts during subduction (e.g., Hoernle et al., 2002; Buchs et al., 2011; Prendergast and Offler, 2012), means that they can be preserved in the geological record, and thus can provide important insights into magmatic and mantle processes in long-destroyed oceans. They also can provide insights into the processes of continental growth at destructive plate margins (Buchs et al., 2016).

The Altaids or Central Asian Orogenic Belt (CAOB) represents one of

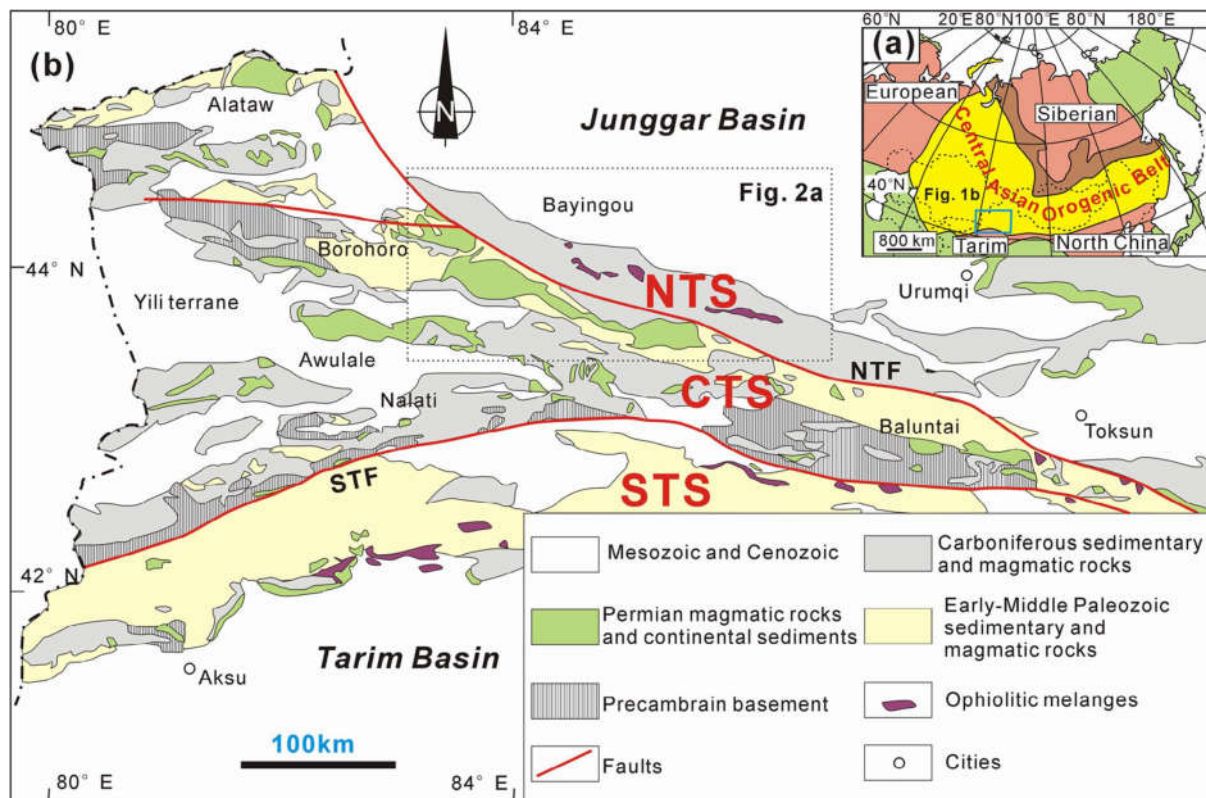


Fig. 1. (a) Overview map showing the Central Asian Orogenic Belt and adjacent cratons. (b) The tectonic geological map of the Chinese Tian Shan. NTS=North Tianshan accretionary complex; CTS =Yili-Central Tianshan block; STS= South Tianshan accretionary complex (modified after Liu et al., 2015).

the largest accretionary orogens in the world and comprises subduction- accretion complexes, arc rocks, ophiolites, seamounts and microcontinents accreted from the Neoproterozoic to the late Phanerozoic, during the closure of the paleo-Asian Ocean (Fig. 1a; Şengör et al., 1993; Windley et al., 2007; Wilhem et al., 2012; Xiao et al., 2015; Yang et al., 2015). The vast accretionary complexes of the CAOB contain a significant proportion of more-enriched basalts (Yang et al., 2015), similar in composition to modern-day ocean island basalts (OIB). On the basis of their geochemistry and nature of associated sediments many of these enriched basalts have been interpreted as the accreted remnants of seamounts (e.g., Safonova and Santosh, 2014; Yang et al., 2012a, 2012b, 2013, 2015). However, since accreted seamounts generally get caught up in ophiolitic mélangé belts they have undergone intense deformation, so can easily be misinterpreted as “classic” ophiolitic units (cf. Khan et al. (2007) and Kakar et al. (2014)). The exceptions are the large seamounts (like the Louisville and Emperor seamounts), which are more likely to be accreted rather than partially subducted, these are, however, rather rare in the geological record (Hauri, 1996). In this paper we present new tectonostratigraphic and geochemical data from accreted seamounts exposed in the North Tianshan accretionary complex (Xiao et al., 2013). Our observations provide convincing evidence for seamount development in the paleo- Asian Ocean, and represent a new opportunity for the study of remnant oceanic intraplate volcanoes in the CAOB.

## 2. Geological background and features of the Bayingou ophiolitic mélangé

As the southern branch of the CAOB, the Tianshan orogenic belt is located between the Junggar and Tarim Basins, and extends E-W about 3000 km from NW China to Kazakhstan

and Kyrgyzstan (Fig. 1b). The Chinese part of the Tianshan orogenic belt is generally divided into eastern and western segments roughly along longitude 88°E (Li et al., 2006). Tectonically, the Western Tianshan orogen can be divided into North Tianshan accretionary complex (NTAC), Yili-Central Tianshan block (CTB) and South Tianshan accretionary complex (STAC) that are bounded by the North Tianshan fault (NTF) and the South Tianshan fault (STF), respectively (Fig. 1b).

The NTAC is located between the Junggar terrane and Yili-Central Tianshan block in the SW of the CAO (Fig. 2a; Zhu et al., 2005; Gao et al., 2009b; Wang et al., 2009; Xiao and Santosh, 2014), and extends over 300 km along the northern edge of the CTB. The NTAC is bounded in the south by the NW–striking North Tianshan fault and in the north by a north-directed thrust that has thrusted the accretionary complex over the Permian and Cretaceous sequences. The accreted sequence predominantly comprises two lithologies: (1) Devonian-Carboniferous volcanosedimentary rocks widely regarded to be an accretionary complex (Wang et al., 2006), and (2) ophiolitic remnants (Gao et al., 1998). The siliceous rocks in the accretionary complex contain Famennian (372–359 Ma) conodonts and Lower Carboniferous radiolarians (Xiao et al., 1992), while gabbro from the Bayingou ophiolitic mélange has

yielded zircon U-Pb ages of  $344 \pm 3$  Ma (Xu et al., 2006a).

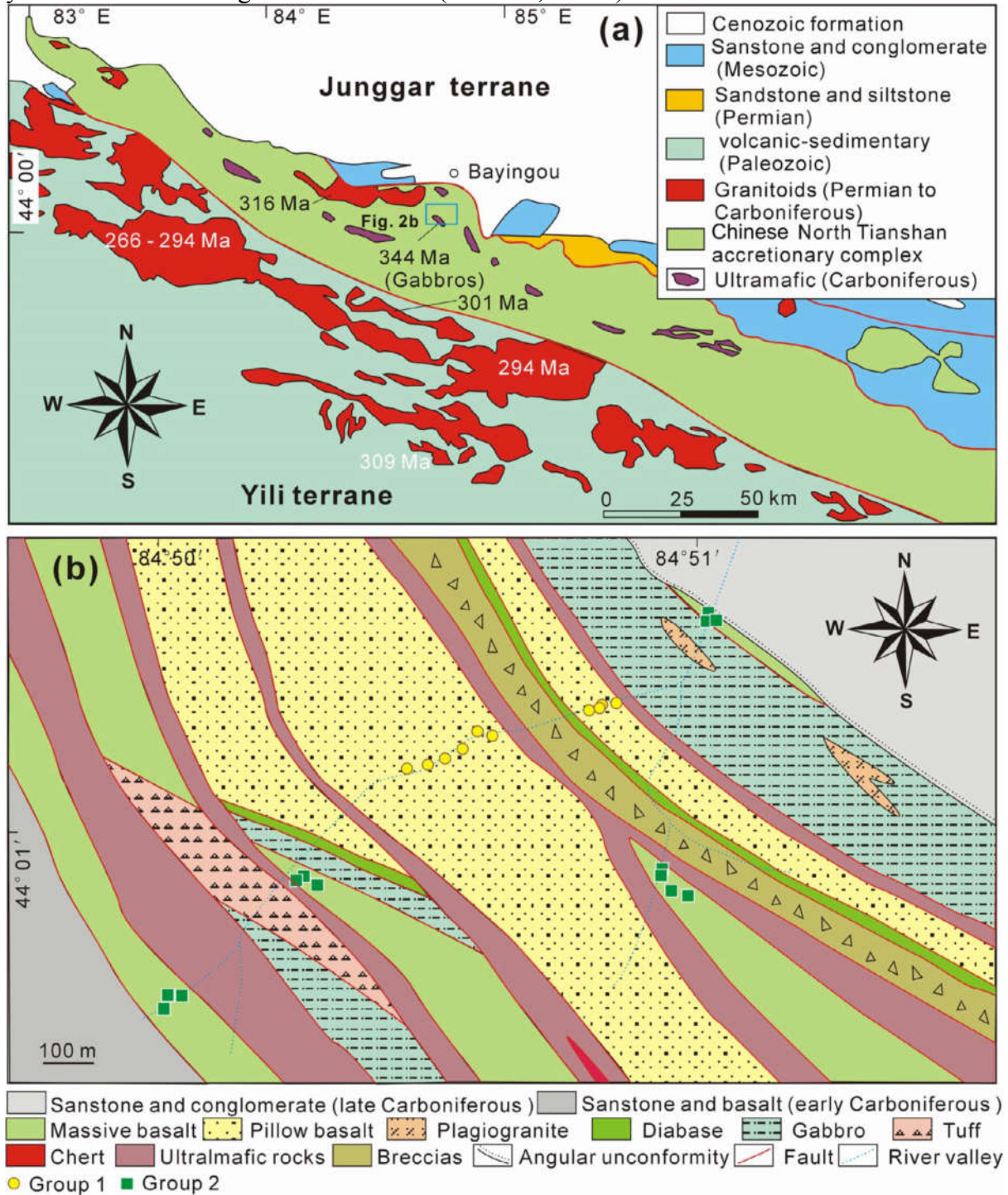


Fig. 2. (a) Tectonic map showing the North Tianshan accretionary complex and adjacent region (modified after Han et al., 2010). (b) Geological map of the Bayingou ophiolitic mélangé (modified after Xu et al., 2006b) and sample locations.

The undeformed Sikeshe granodiorite, K-feldspar granite and diorite pluton that intruded into flysch has been dated by SHRIMP zircon U-Pb at  $316 \pm 3$  Ma (Han et al., 2010).

The CTB is suggested to represent a composite arc terrane that developed on a Precambrian basement (Gao et al., 2009a), which consists of the Precambrian amphibolite- and granulite-facies metamorphic rocks (Liu et al., 2004; Shu et al., 2004). Ordovician–Silurian

metavolcanic-sedimentary rocks are fault contact with the Precambrian basement, and are overlain unconformably by non-metamorphosed the Lower Carboniferous sedimentary rocks (Gao et al., 1998; Charvet et al., 2011). The volcanic rocks interbedded within the Paleozoic sediments have subduction-related geochemical features (Che et al., 1994; Zhu et al., 2005, 2009; Li et al., 2010, 2017). The granitoids, which are widely distributed and intruded into the Proterozoic to Paleozoic volcanic-sedimentary rocks, are mainly composed of adamellite, moyite, diorite and quartz diorite with different ages (Tang et al., 2010; Long et al., 2011; Dong et al., 2011; Ma et al., 2014; Wang et al., 2015; Zhong et al., 2015). Moreover, several ophiolitic mélanges have

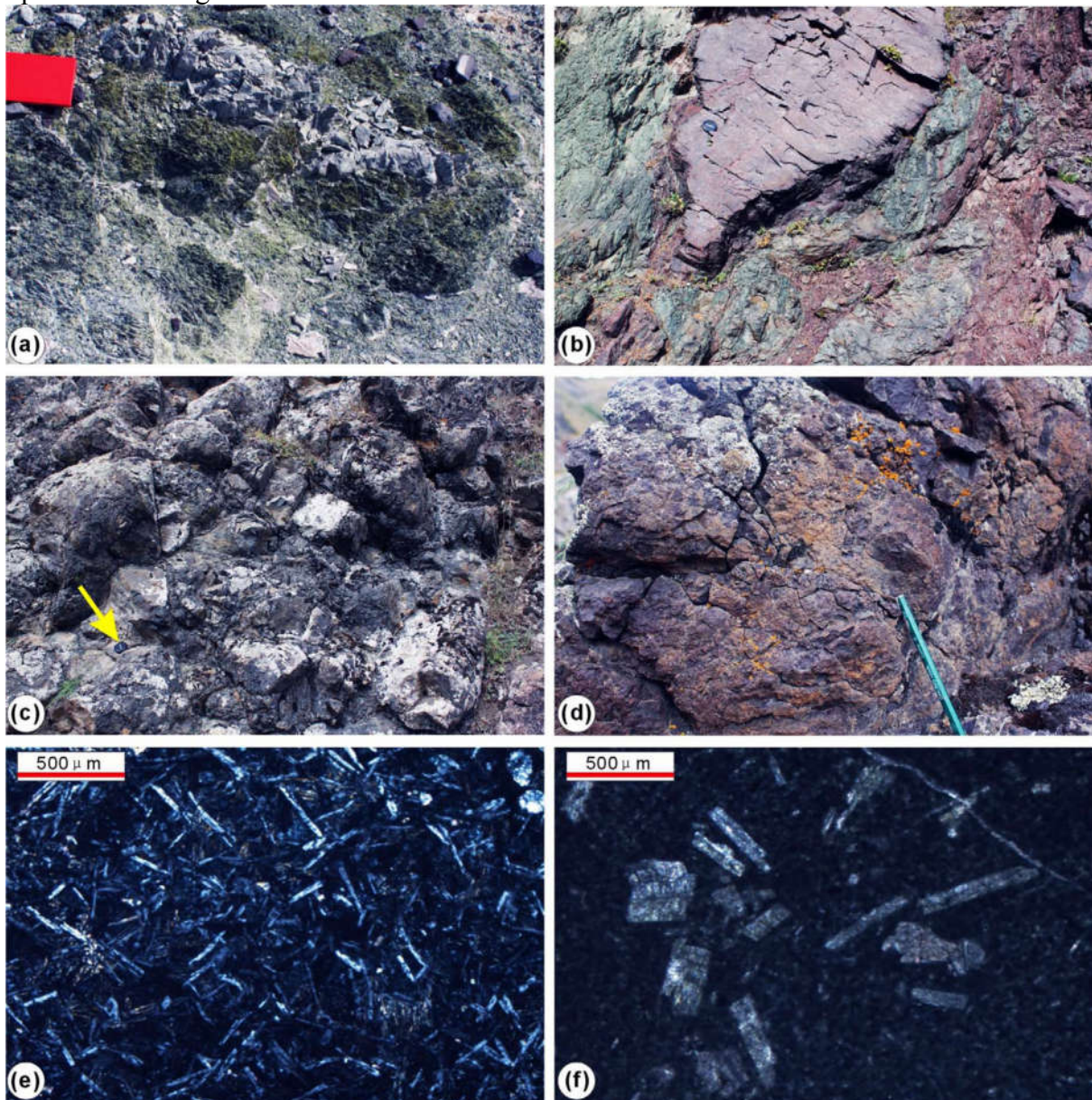


Fig. 3. Field photographs of typical outcrops and photomicrographs from the Bayingou ophiolitic mélangé in the North Tianshan accretionary complex. (a) Metagabbros in ultramafic rocks with cleavages. (b) Chert lens occurring in tuffs. (c) Pillow basalts from Group 1 with interstratified tuffs. (d) Massive basalts in the field (Group 2). (e) Equigranular textures in pillow basalts (cross-polarised light, group 1). (f) Typical porphyritic texture in massive basalts (cross-polarised light, group 2).

been recognized in the CTB, such as the Bingdaban, Mishigou and Gangou ophiolitic mélanges (Charvet et al., 2007; Dong et al., 2006, 2007).

The STAC marks the suture between the Yili-Central Tianshan block and the Tarim Basin (Xiao et al., 2013; Jiang et al., 2014), and consists predominantly of the Lower Cambrian black shales and phosphoric silicates, Cambrian–Carboniferous marine/non-marine carbonates, clastic rocks, cherts and interlayered volcanics (Allen et al., 1992; Carroll et al., 1995). Several ophiolitic mélanges with ages ranging from 450 Ma to 332 Ma developed in the STAC (Gao et al., 1998; Wang et al., 2007; Jiang et al., 2014). Subduction- and/or collision-related high-pressure/low-temperature metamorphism is also preserved (Gao et al., 1998; Zheng et al., 2006; Lü et al., 2008). Moreover, large volume Late Carboniferous to Permian syn- and post-collisional granitic plutons are found intruding the STAC (Konopelko et al., 2009; Long et al., 2011; Han et al., 2011; Gou et al., 2012).

The Bayingou ophiolitic mélange is exposed discontinuously over an area ~250 km in length by 5–15 km in width (Fig. 2b), and consists of strongly serpentinised ultramafic rocks (including harzburgite, lherzolite, pyroxenite, dunite and peridotite), as well as pillowed and massive basalts, layered gabbros, radiolarian cherts, pelagic limestones, breccias and tuffs. These rocks show a series of tight isoclinal folds and display block-in-matrix structures (Figs. 3a and b). The blocks range from tens of centimeters to several hundreds of meters and are set in a matrix of serpentinised ultramafic rocks, basalts and tuffs. In most cases the matrix is strongly sheared so that a scaly fabric is developed in weakly metamorphosed pelite. Harzburgite, one of the main ultramafic rocks, contains more than 70% olivine, 15% clinopyroxene, 5% orthopyroxene, and about 5% spinel. Dunite, another main ultramafic rock, contains more than 95% olivine, 5% of orthopyroxene. However, both ultramafic rocks are strongly serpentinised with a net-like texture of chrysotile and antigorite with only a few relicts of fresh olivine and enstatite being preserved.

Gabbro occurs mainly as blocks but small sheet-like layered intrusions are preserved in some places, and mainly consist of clinopyroxene and plagioclase, as well as ilmenite, magnetite, sphene

**Table 1**  
Major element compositions of basalts from the Bayingou ophiolitic mélange.

Sample	Type	SiO <sub>2</sub>	TiO <sub>2</sub>	Al <sub>2</sub> O <sub>3</sub>	Fe <sub>2</sub> O <sub>3</sub>	MnO	MgO	CaO	Na <sub>2</sub> O	K <sub>2</sub> O	P <sub>2</sub> O <sub>5</sub>	LOI	Total
BY-1	Group 1	50.58	2.23	14.46	10.30	0.13	6.76	8.97	5.15	0.13	0.34	0.90	99.95
BY-2		50.17	2.77	14.82	10.87	0.12	5.59	8.39	6.00	0.13	0.40	0.60	99.86
BY-3		51.58	2.53	13.56	9.90	0.17	6.96	7.62	5.74	0.15	0.52	1.10	99.83
BY-4		49.39	2.89	13.52	11.12	0.21	6.87	8.15	5.57	0.15	0.43	1.24	99.54
BY-5		49.56	2.89	13.78	11.21	0.15	6.82	7.95	5.65	0.16	0.54	1.08	99.79
BY-6		51.12	2.76	14.49	9.87	0.22	6.17	7.86	5.57	0.15	0.53	1.08	99.82
BY-7		51.32	2.44	14.21	10.32	0.19	6.23	8.34	5.21	0.14	0.41	1.12	99.93
BY-8		50.72	2.68	13.89	11.13	0.17	6.15	8.14	5.28	0.16	0.48	1.21	100.01
BY-9		49.38	2.53	14.77	10.30	0.16	6.76	8.97	5.15	0.15	0.47	1.25	99.89
BY-10		50.22	2.81	14.22	10.62	0.19	5.78	8.18	5.89	0.16	0.47	1.18	99.72
BY-11	Group 2	49.96	1.33	13.97	15.53	0.24	4.79	6.70	5.14	0.70	0.20	1.37	99.93
BY-12		49.00	0.84	14.61	11.21	0.16	8.85	10.44	2.65	0.54	0.07	1.44	99.81
BY-13		50.59	0.88	14.01	11.35	0.18	9.01	9.99	3.65	0.10	0.07	0.50	100.33
BY-14		49.55	0.84	14.13	11.22	0.16	8.79	10.87	3.08	0.29	0.07	0.94	99.94
BY-15		49.97	1.68	13.10	16.88	0.18	4.29	5.96	5.99	0.45	0.28	0.95	99.73
BY-16		50.97	1.23	15.60	13.41	0.17	4.24	6.17	6.79	0.12	0.13	0.87	99.70
BY-17		50.46	1.25	15.37	13.55	0.17	4.99	5.92	6.46	0.48	0.18	1.12	99.95
BY-18		49.07	1.19	16.78	13.16	0.28	5.25	6.59	5.23	2.03	0.31	0.22	100.11
BY-19		48.19	1.13	16.00	11.52	0.22	6.37	10.39	3.34	1.89	0.11	0.83	99.99
BY-20		51.54	1.41	14.22	9.78	0.24	5.48	10.08	5.13	1.00	0.10	0.87	99.85
BY-21		50.62	1.98	14.07	14.52	0.21	6.00	5.07	5.89	0.41	0.28	0.65	99.70
BY-22		45.14	1.13	13.32	14.46	0.22	6.22	8.99	9.73	0.44	0.22	0.23	100.10
BY-23		50.50	1.53	13.90	13.84	0.21	5.61	5.96	6.76	1.04	0.15	0.61	100.11

and zircon. Plagioclase is usually enclosed by clinopyroxene which has a poikilitic texture. Gabbros have undergone low temperature metamorphism to hornblende, actinolite, epidote and chlorite. The basalts can be divided into two types: pillowed (Fig. 3c and e) and massive (Fig. 3d and f). The pillowed basalt occurs extensively as blocks in the Bayingou area, and

contains amygdales that are filled with chalcedony or calcite. The pillowed basalts also display a porphyritic texture with clinopyroxene and plagioclase phenocrysts in groundmass of finegrained plagioclase, clinopyroxene and opaque minerals. The groundmass plagioclase has a quench texture which is unique feature of marine volcanic rocks (Peng et al., 2005). The massive basalt occurs as not only matrix but also blocks in the mélange, and shows an interstitial texture as well as a porphyritic texture. These basalts are composed of plagioclase, clinopyroxene, magnetite, ilmenite, and minor zircon, and also shows low-grade metamorphism with albite, epidote, chlorite, and calcite. In previous regional studies, the mafic rocks of the Bayingou ophiolitic mélange were suggested to belong to three different geochemical groups: N-MORB, OIB and island arc tholeiite (IAT) (Wu and Liu, 1989; Xiao et al., 1992; Xu et al., 2006b; Chen et al., 2012). Chert is generally juxtaposed against massive and pillowed basalt, and has undergone multiple folding and thrusting. Bedded pelagic limestone is found along with massive and pillowed basalt, chert, and tuff, and occurs mostly as blocks in a matrix of turbidite.

### 3. Analytical methods

In order to determine the composition of the seamounts, 23 wholerock samples of basalts were selected for X-ray fluorescence (XRF) and inductively coupled plasma–mass spectrometry (ICP-MS) analyses at the Chang'an University (China). Analytical procedures are similar to those described by Li et al. (2006). Based on the analysis of international reference materials and duplicate samples, the analytical errors for the major elements were about 1–2 wt.% for SiO<sub>2</sub>, Al<sub>2</sub>O<sub>3</sub>, TiO<sub>2</sub>, Fe<sub>2</sub>O<sub>3</sub> and MgO and less than 3 wt.% for the other oxides. About 50 mg of each powdered sample was dissolved in a high-pressure Teflon bomb for 24 h using a HF+ HNO<sub>3</sub> mixture. International reference material (BE-N) was used to monitor data quality during the course of this study. The precision and accuracy of the trace element analyses are estimated to be better than 5 wt.% (relative), except for Nb and Ta (better than 10 wt.%). For detailed information see appendix Table 1.

The isotope ratios of Nd, Sr and Pb along with associated isotope– dilution concentrations were measured at the Test and Research Center, Beijing Nuclear Industry Geological Research Institute, China. <sup>87</sup>Sr/<sup>86</sup>Sr and <sup>143</sup>Nd/<sup>144</sup>Nd ratios were measured on a MAT-261 mass spectrometer, and isotopic ratios were normalised to <sup>146</sup>Nd/<sup>144</sup>Nd = 0.7219 and <sup>86</sup>Sr/<sup>88</sup>Sr = 0.1194. Repeat analyses yielded averages of 0.710236 ± 0.000007 (2σ, n = 6) for Sr standard NISTSRM987, and 0.511864 ± 0.000003 (2σ, n = 6) for the La Jolla Nd standard. Total elemental blanks were <200 pg for Sr and <100 pg for Nd. For whole rock Pb isotopic compositions, about 100 mg powder was accurately weighed into a Teflon beaker, spiked and digested in concentrated HF at 180 °C for 7 h. Lead was separated and purified by using AG1×8, 20–400 cation-exchange resin with dilute HBr as an eluant. Total procedural blanks were <50 pg Pb. Lead isotopic ratios were measured using a VG-354 mass-spectrometer. Repeat analyses of SRM 981 yielded average values of <sup>206</sup>Pb/<sup>204</sup>Pb = 16.9325 ± 3 (2σ), <sup>207</sup>Pb/<sup>204</sup>Pb = 15.4853 ± 3 (2σ) and <sup>208</sup>Pb/<sup>204</sup>Pb = 36.6780 ± 9 (2σ). External precision for the Pb isotope systems are less than 0.005, 0.005 and 0.0015, respectively.

### 4. Results

As detailed in Section 2, most of the samples are quite altered (principally to chlorite and epidote) and so have undergone significant post-magmatic fluid-rock interaction. However, they have relatively low loss on ignition values (LOI < 1.37 wt.%; Table 1). Despite these low LOI values hydrothermal alteration is likely to have mobilised some of the major elements and the large ion lithophile (LIL) elements (Ba, Rb, Sr, and K), as has been

documented in numerous studies (e.g., Pearce, 1996; Polat and Hofmann, 2003). However, the high field- strength (HFS) elements such as Nb, Ta, Zr, Hf, Y and Th are generally regarded to be relatively immobile during low-temperature alteration (e.g., Pearce and Cann, 1973; Polat et al., 2002). Although Sr isotopes can be significantly affected by interaction with high  $^{87}\text{Sr}/^{86}\text{Sr}$  seawater (e.g., Kawahata et al., 2001; Godard et al., 2006), Nd and Pb radiogenic isotope ratios are relatively insensitive to alteration and are much more reliable indicators of magmatic sources (Rodrigo-Gámiz et al., 2015; Simon et al., 2017). We therefore use immobile trace elements along with Nd and Pb radiogenic isotope ratios as well as field observations and regional constraints in our assessment of the petrogenesis and tectonic setting of these rocks.

Two distinct compositional groups are evident within the geochemically heterogeneous Bayingou ophiolitic mélange (Fig. 4). Group 1 have MgO ranging from 5.6 to 7.0 wt.% and are characterised by high

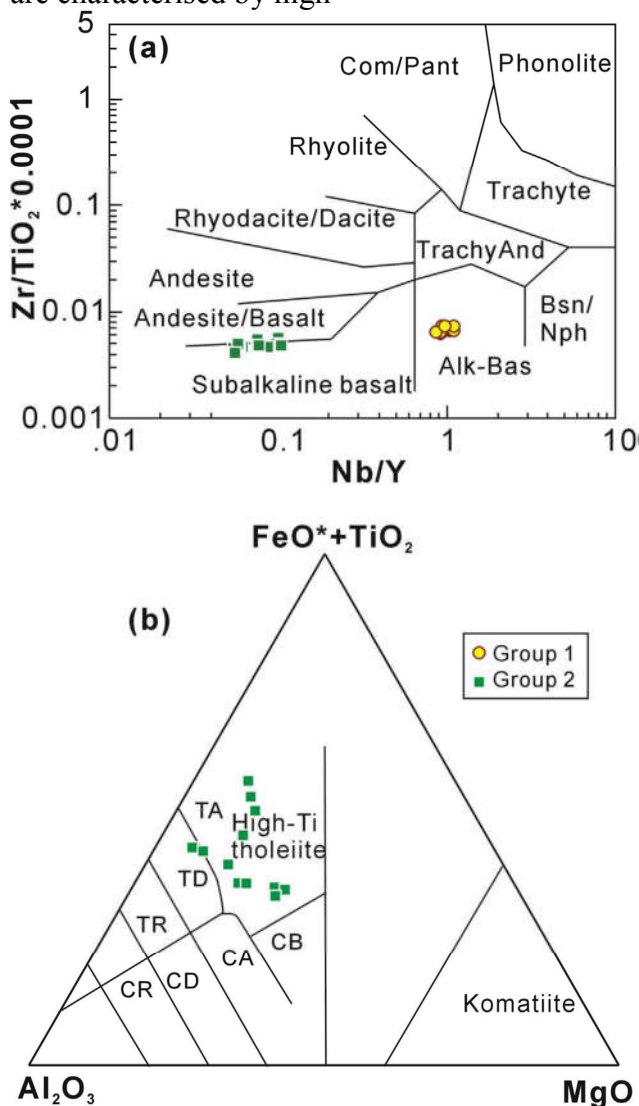


Fig. 4. Geochemical classification diagrams for the basaltic units in the Bayingou ophiolitic mélange in the North Tianshan accretionary complex. (a)  $\text{Zr}/\text{TiO}_2$  versus  $\text{Nb}/\text{Y}$  (after Winchester and Floyd, 1977). (b)  $\text{Al}_2\text{O}_3$ – $\text{FeO} + \text{TiO}_2$ – $\text{MgO}$  diagram (Jensen, 1976); tholeiitic series: TA - andesite, TD - dacite, TR - rhyolite; calc-alkaline series: CB - basalt, CA - andesite, CD - dacite, CR - rhyolite; kom - komatiite.

concentrations of TiO<sub>2</sub> (2.2–2.9 wt.%, Table 1). Magnesium number (Mg# = molar Mg<sup>2+</sup>/[Mg<sup>2+</sup>+Fe<sup>2+</sup>], assuming 85% of total Fe is Fe<sup>2+</sup>) varies from 51 to 59. Group 1 samples have a restricted compositional range, and do not show a clear linear relationship with increasing MgO (Fig. 5). In contrast, P<sub>2</sub>O<sub>5</sub>, Cr and Ni in Group 1 samples range to higher values than in Group 2 (Table 2). However, Al<sub>2</sub>O<sub>3</sub> range to lower than in Group 2 (Fig. 5).

These rocks classify as alkaline basalts on an immobile element (Zr-Ti-Nb-Y) classification plot (Fig. 4a). This alkaline affinity is also evidenced by light rare earth element (LREE) enrichment and heavy rare earth element (HREE) depletion (Fig. 6a, (La/Yb)<sub>N</sub>=5.9–7.5, N - Chondrite normalised). Group 1 samples also show slight negative Zr-Hf anomalies and have a similar trace element signature to ocean island basalt (OIB) (Fig. 6b, Fig. 7). The rocks of this group have a very restricted range of Nd-Pb isotopic compositions ( $\epsilon$ Nd(t)=+5.8–+7.0, <sup>206</sup>Pb/<sup>204</sup>Pb=19.39–19.53; <sup>207</sup>Pb/<sup>204</sup>Pb=15.71–15.73; <sup>208</sup>Pb/<sup>204</sup>Pb=40.03–40.21; Tables 3 and 4). The basalts have lower  $\epsilon$ Nd(t) and <sup>208</sup>Pb/<sup>204</sup>Pb for a given <sup>206</sup>Pb/<sup>204</sup>Pb, than the Society and Cook-Austral islands and the Louisville Seamount Chain but overlap with the field for the Hawaiian basalts. The samples plot close to the DMM end member and seem to fall on a trend between depleted mantle and EM1 (Fig. 8). Although Sr isotopic compositions span a relatively small range (<sup>87</sup>Sr/<sup>86</sup>Sr=0.70493–0.70511), they do not look like magmatic values and are probably influenced by seawater alteration as mentioned above.

Group 2 basaltic rocks (4.3–9.0 wt.% MgO) have a much more incompatible element-depleted (MORB-like) signature (Fig. 6a) with LREE depletion (La/Sm)<sub>N</sub>= 0.5–0.9; N - Chondrite normalised) and essentially flat HREE patterns (Dy/Yb)<sub>N</sub>= 0.9–1.2; N - Chondrite normalised). They are also characterised by lower concentrations of TiO<sub>2</sub> (0.9–2.0 wt.%) and a greater variation in Mg# (34–62) than Group 1, again with no significant negative Nb, Ta or Ti anomalies (Fig. 6b). This group are much more tholeiitic in nature (Fig. 4b) and straddle the boundary between basaltic andesite and sub-alkaline basalt on an immobile element (Zr-Ti-Nb-Y) classification plot (Fig. 4a). This more tholeiitic nature is also consistent with the depleted MORB-like trace element signature (Fig. 7). Despite their trace element-depleted signature of Group 2 has slightly more enriched  $\epsilon$ Nd(t) (3.2–4.4; Table 3) and lower initial <sup>206</sup>Pb/<sup>204</sup>Pb (18.28–18.48), <sup>207</sup>Pb/<sup>204</sup>Pb (15.51–15.57), and <sup>208</sup>Pb/<sup>204</sup>Pb (38.43–38.60) compared to those of Group 1 (Fig. 8, Table 4). The spread in Sr isotope values along with a relatively small range in Nd and Pb implies that Sr isotopes have been affected by seawater alteration. These samples fall along the same trend between DMM and EM1 as Group 1 samples but, paradoxically, the more incompatible trace-element depleted Group 2 plot closer to the compositional field of EM1 than the more trace element-enriched Group 1 samples (Fig. 8).

## 5. Discussion

### 5.1. Source nature

As shown in Section 4, their geochemistry indicates that Group 1 have OIB-like trace element normalised patterns (Fig. 6) with (La/Yb)<sub>N</sub> ratios >6 (Table 2). Immobile element ratios and discrimination diagrams (Figs. 7 and 9) further suggest that they have formed in a within plate setting. The association of the basalts with marine sediments indicates they did not erupt in a continental setting, but rather formed in an ocean basin and so are probably the result of mantle plume-related magmatism. La/Sm (3.3–3.9) and Th/Yb (1.1–1.4) values for Group 1 are extremely high, similar to the Hawaii and Louisville basalts (Fig. 7a), suggesting

that they were generated through

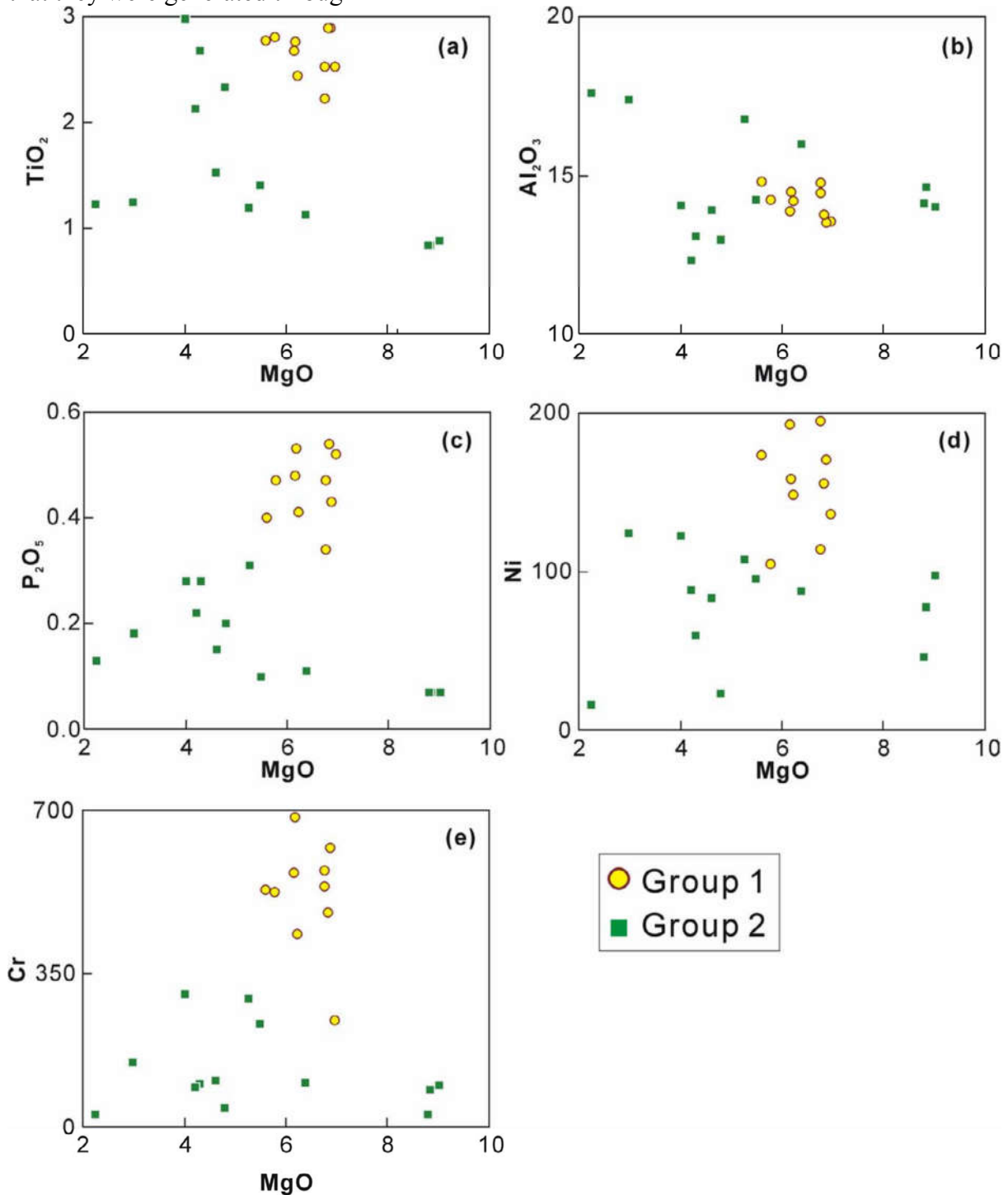


Fig. 5. Representative variation diagrams of major and trace element compositions versus MgO for the basalts in the Bayingou ophiolitic mélangé.

small degrees of melting of a mantle source. Samples in Group 1 are consistently slightly more enriched in LREE relative to Group 2. The geochemistry indicates that Group 2 have MORB-like trace element normalised patterns (Fig. 6) with (La/Yb)<sub>N</sub> ratios < 1 (Table 2). However, immobile element ratios and discrimination diagrams (Figs. 7 and 9) suggest that they have formed in mid-oceanic ridge setting but interacted with a more-enriched plume source. Therefore, it is likely that both groups owe their origin to melting of a mixture between plume and depleted MORB mantle.

Pooled fractional melt calculations have been used to model the composition (depleted vs. primitive mantle) and mineralogy (lherzolite containing either spinel or garnet or a 50:50 mix representing melting across the transition zone) of the source region (Aldanmaz et al., 2006; Kerr et al., 2004, 2009). Partition coefficients are averages from Salters et al. (2002) and McDade et al. (2003). Mantle mineral proportions and source compositions have been taken from McKenzie and O'Nions (1991).

The melt modelling suggests that the higher (La/Nd)<sub>cn</sub> ratios of Group 1 are consistent with a slightly more enriched source region (Fig. 10a). Group 1 samples all plot between the 50:50 garnet–spinel lherzolite and spinel lherzolite melt model curves, indicating that the source contains some garnet. The modelling further suggests that Group 1 lavas formed by relatively small (2–5%) degrees of mantle melting. In contrast, although the basalts in Group 2 have a more enriched isotopic signature, their depleted LREE and flat-HREE signatures are better modelled using a depleted shallower spinel lherzolite mantle source composition, that has undergone 10–20% melting.

It is therefore likely that Group 2 basalts, with incompatible element ratios that are mostly similar to MORB (Fig. 9) yet have radiogenic isotope compositions that are more enriched than Group 1, are derived from a mantle source that has undergone a previous melting episode. Since this depletion is not recorded in the isotopic signatures it is clear that this previous melting event occurred shortly before the formation of the Group 2 basalts and does

not indicate a long-term source

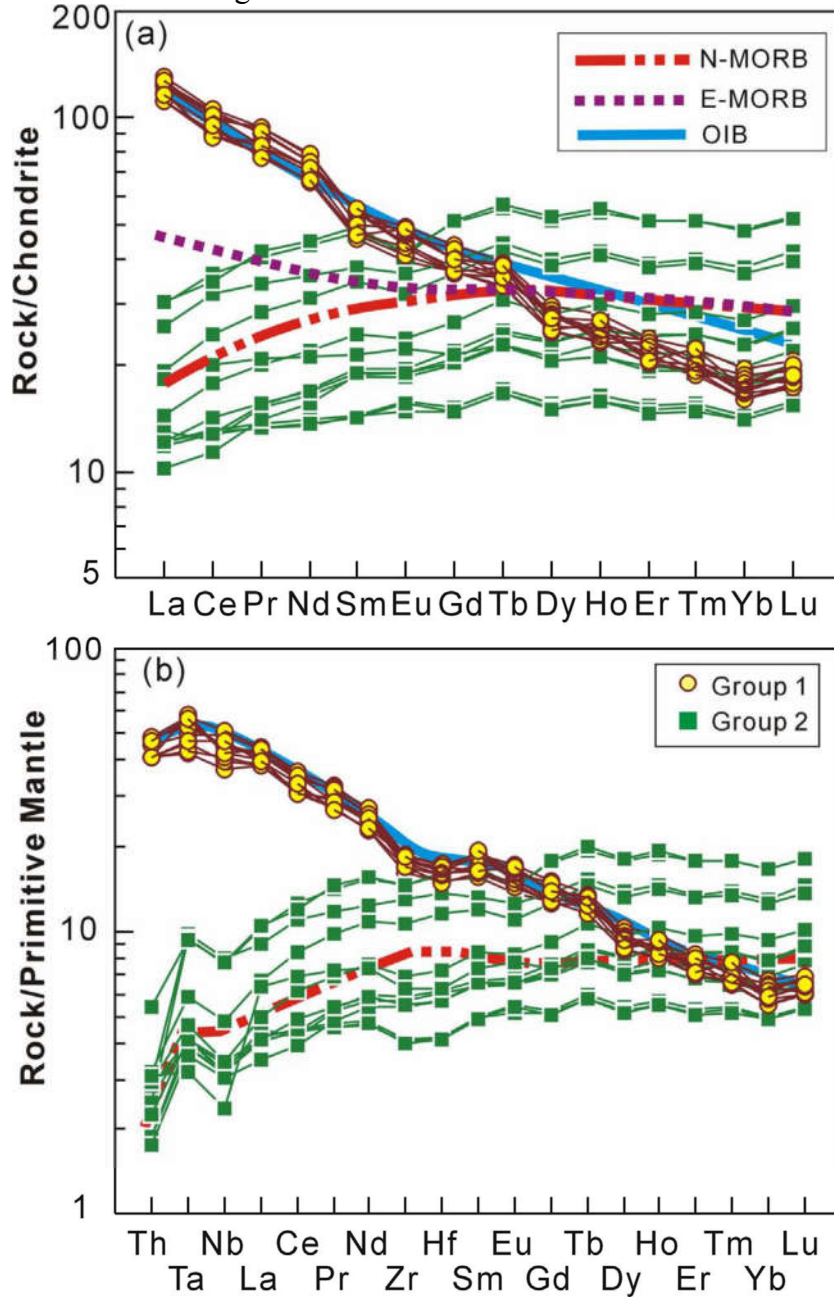


Fig. 6. (a) Chondrite-normalised rare earth element and (b) primitive mantle-normalised trace-element patterns for the basalts in the Bayingou ophiolitic mélange. The normalising values, E-MORB, OIB and N-MORB compositions are from Sun and McDonough (1989).

depletion. On all the isotope plots involving Pb and Nd, both groups of basalts lie on clear mixing trends between depleted MORB Mantle (DMM) and EM1, with Group 2 consistently plotting closer to EM1 than Group 1 (Fig. 8). The involvement of an enriched mantle source in the formation of Group 2 basalts (and to a lesser extent Group 1 basalts) along with the associated occurrence of pelagic sedimentary rocks support formation in an intra-oceanic setting. The fact that, both groups lie along a DMM-EM1 mixing line (Fig. 8) suggests that they may be genetically related.

## 5.2. Petrogenesis of basalts

It is generally assumed that the OIB are derived from mantle plumes and that these magmas commonly have more enriched compositions than MORB (Hofmann, 1997). Recent discoveries indicate that enriched basalts are not only limited to mantle plumes but can be found in oceanic spreading ridges (Niu et al., 2002; Hemond et al., 2006; Nauret et al., 2006), and in some arc-related settings (Kita et al., 2001; Scott et al., 2002) such as slab roll-back (Ferrari et al., 2001), arc rifting (Mueller et al., 2002) and deep water cycle model (Ivanov and Litasov, 2014). Moreover, Hirano et al. (2006) proposed that the small alkaline volcanoes erupt along lithospheric fractures in response to plate flexure

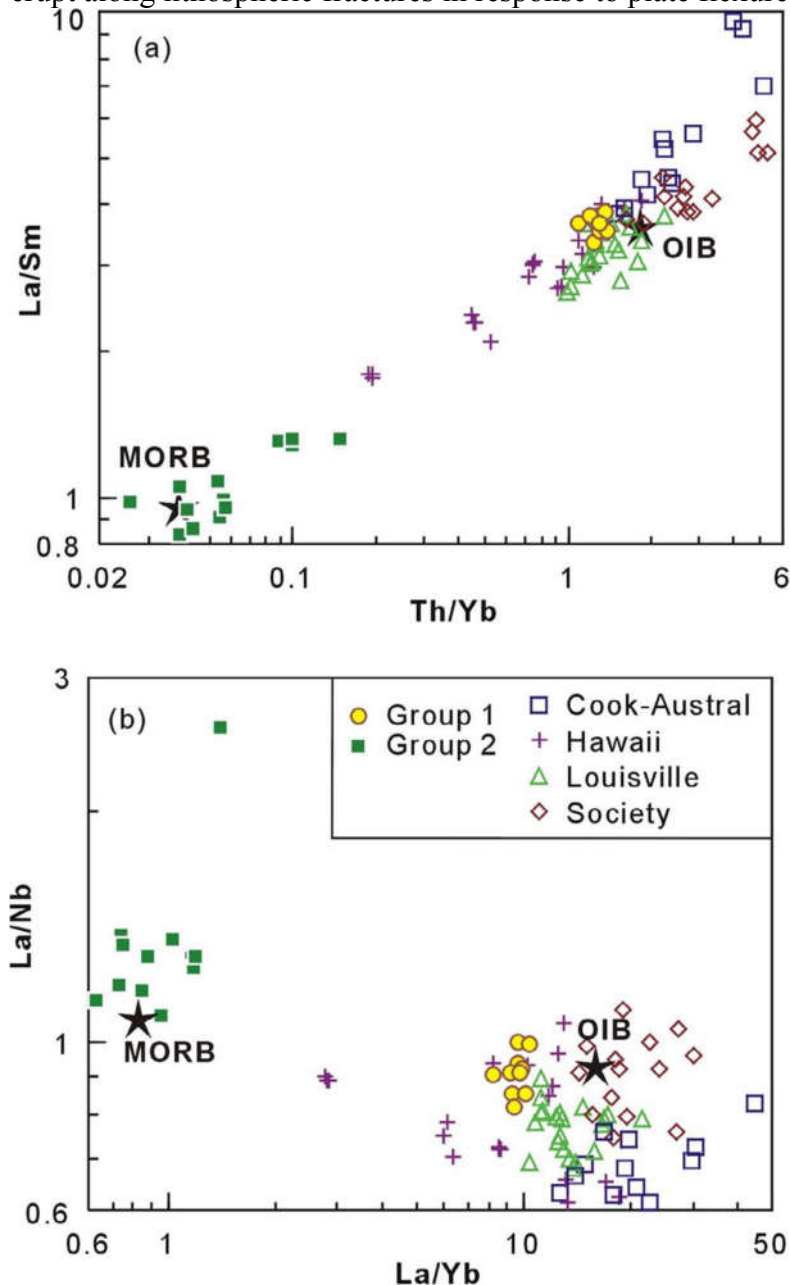


Fig. 7. Plots of (a) Th/Yb versus La/Sm, and (b) La/Yb versus La/Nb for the basalts in the Bayingou ophiolitic mélange. Data sources: Cook–Austral from Lassiter et al. (2003), Hawaii from Huang et al. (2005), Society from White and Duncan (1996), Louisville from Vanderkluyesen et al. (2014), OIB and MORB compositions are from Sun and McDonough (1989).

during subduction. In our previous studies we discussed the occurrences of alkaline basalts hosted by ophiolitic mélanges in the West Junggar and suggested that the plume-related magmatism developed during the evolution of the Junggar ocean as well as paleo-Asian

Ocean (Yang et al., 2012b, 2013, 2015). Safonova and Santosh (2014) also considered that the OIB-bearing units of the CAOB and the Western Pacific formed in relation to two superplumes: the Asian with age of the Late Neoproterozoic and the Pacific with age of the Cretaceous. Moreover, Fitton et al. (1997) have successfully developed the robust  $\Delta Nb$  approach ( $\Delta Nb = 1.74 + \log(Nb/Y) - 1.92 \times \log(Zr/Y)$ ) to identify the mantle source of mafic rocks. Mafic magmas derived from plume exhibit  $\Delta Nb > 0$ , whereas magmas derived from depleted mantle and the crust show  $\Delta Nb < 0$  (Fitton et al., 1997; Baksi, 2001). The Group 1 basalts have  $\Delta Nb$  values ranging from 0.18 to 0.28, showing a geochemical signature (Table 2) consistent with a mantle plume origin. However, Group 2 basalts have  $\Delta Nb$  values ranging from 0.25 to 0.11, indicating mixing between plume and MORB mantle sources. This is compatible with both groups plotting on the DMM-EM1 mixing line (Fig. 8).

**Table 4**  
Pb isotope compositions of basalts from the Bayingou ophiolitic mélange in the North Tianshan.

Sample	Type	U	Th	Pb	$^{238}\text{U}/^{204}\text{Pb}$	$^{235}\text{U}/^{204}\text{Pb}$	$^{232}\text{Th}/^{204}\text{Pb}$	$^{206}\text{Pb}/^{204}\text{Pb}$	$^{207}\text{Pb}/^{204}\text{Pb}$	$^{208}\text{Pb}/^{204}\text{Pb}$	$(^{206}\text{Pb}/^{204}\text{Pb})_i$	$(^{207}\text{Pb}/^{204}\text{Pb})_i$	$(^{208}\text{Pb}/^{204}\text{Pb})_i$
BY-1	Group 1	0.75	3.46	1.97	27.00	0.196	125.45	19.53	15.73	40.21	18.05	15.65	38.06
BY-2		0.91	4.1	2.1	30.73	0.223	139.46	19.39	15.71	40.04	17.71	15.62	37.64
BY-3		0.77	3.48	2.01	27.16	0.197	123.67	19.49	15.73	40.14	18.00	15.65	38.01
BY-4		0.73	3.51	1.92	26.96	0.196	130.58	19.39	15.72	40.16	17.91	15.64	37.91
BY-5		0.82	3.49	2.05	28.36	0.206	121.60	19.51	15.72	40.13	17.96	15.64	38.04
BY-6		0.83	4.05	1.96	30.03	0.218	147.59	19.49	15.71	40.03	17.84	15.63	37.50
BY-7		0.91	4.1	1.98	32.59	0.236	147.91	19.44	15.73	40.20	17.65	15.63	37.66
BY-8		0.78	3.98	2.03	27.25	0.198	140.04	19.53	15.72	40.20	18.03	15.64	37.79
BY-9		0.82	3.47	2.11	27.56	0.200	117.47	19.45	15.72	40.15	17.94	15.64	38.13
BY-10		0.88	3.87	1.96	31.84	0.231	141.03	19.40	15.72	40.16	17.66	15.62	37.74
BY-11	Group 2	0.07	0.25	1.45	3.23	0.023	12.32	18.43	15.52	38.56	18.25	15.51	38.35
BY-12		0.052	0.22	0.92	4.03	0.029	17.06	18.48	15.52	38.60	18.26	15.51	38.31
BY-13		0.069	0.24	0.31	15.72	0.114	55.70	18.48	15.51	38.44	17.62	15.46	37.48
BY-14		0.058	0.24	0.29	14.07	0.102	57.69	18.28	15.52	38.43	17.51	15.48	37.43
BY-15		0.13	0.21	0.69	12.89	0.093	21.74	18.48	15.57	38.53	17.77	15.53	38.16
BY-16		0.16	0.16	1.01	11.24	0.082	11.57	18.45	15.51	38.44	17.83	15.47	38.24
BY-17		0.17	0.16	0.87	13.74	0.100	13.42	18.36	15.53	38.46	17.60	15.49	38.23
BY-18		0.12	0.15	0.65	12.86	0.093	16.51	18.36	15.56	38.57	17.66	15.52	38.28

The unit for the contents of trace elements (U, Th, and Pb) is  $10^{-6}$ . The isotopic ratios  $^{238}\text{U}/^{204}\text{Pb}$ ,  $^{235}\text{U}/^{204}\text{Pb}$ , and  $^{232}\text{Th}/^{204}\text{Pb}$  are calculated from the measured whole rock U, Th, and Pb contents and the present Pb isotopic compositions.

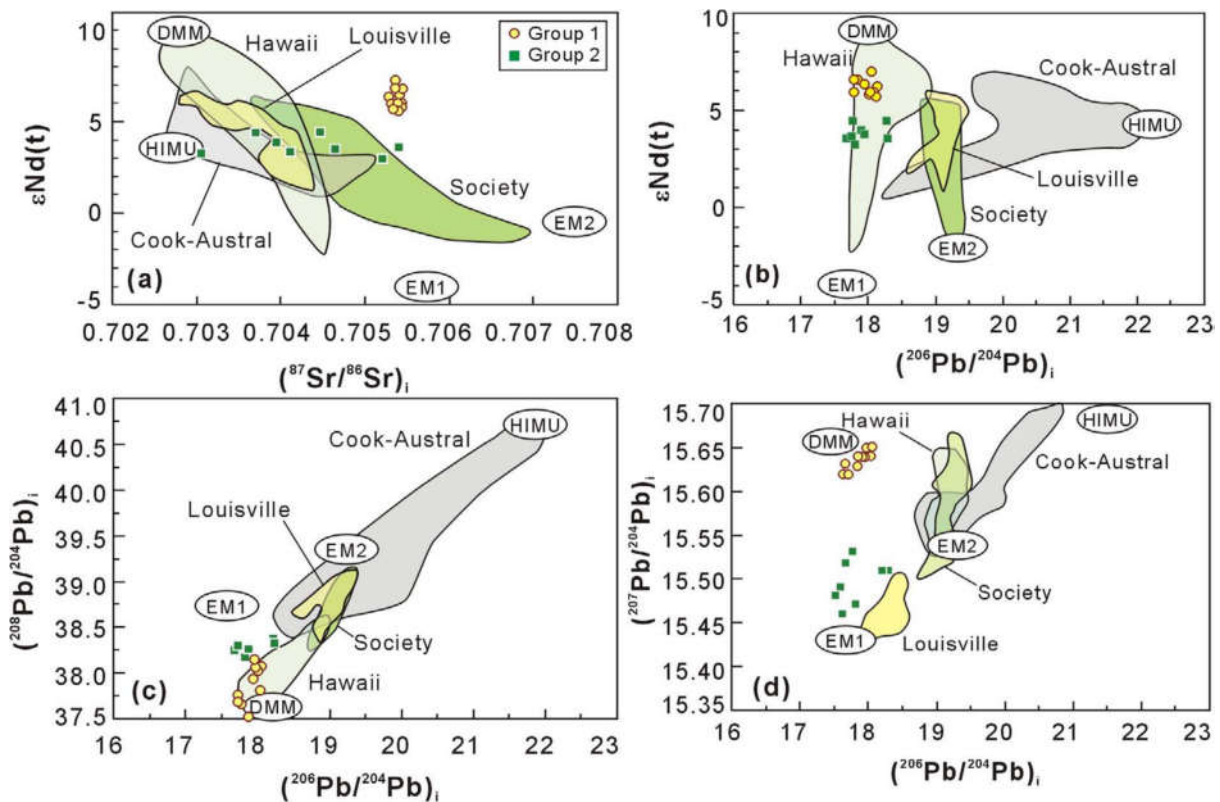


Fig. 8. Age-corrected Sr, Nd and Pb isotopic ratios of basalts in the Bayingou ophiolitic mélangé. The coloured fields enclose present-day values for four other Pacific hot spot islands or island groups. Boxes marked DMM, HIMU, EM1, and EM2 indicate the postulated mantle end-member components of Zindler and Hart (1986). DMM—depleted mid-oceanic ridge basalt mantle, HIMU—high Th/U mantle, EM1—enriched mantle with low  $\epsilon\text{Nd}(t)$  and  $206\text{Pb}/204\text{Pb}$ , and intermediate initial  $87\text{Sr}/86\text{Sr}$ , EM2—enriched mantle with intermediate  $\epsilon\text{Nd}(t)$ , and high  $206\text{Pb}/204\text{Pb}$  and initial  $87\text{Sr}/86\text{Sr}$ . Data sources: See Fig. 7.

As mentioned above, the geochemical attributes of both groups imply no arc-related signatures, however, there are some contemporary arc-related magmas in North Tianshan accretionary complex (Wang et al., 2007; An et al., 2013; Xie et al., 2016). Furthermore, if both groups formed at oceanic spreading ridges, enriched basalts such as EMORB should also be found (Hemond et al., 2006; Nauret et al., 2006). However, there are no documented rocks with an E-MORB signature in this region. Therefore, we infer both groups were derived from a mantle plume, with varying degrees of previous melt extraction from their sources along with likely mixing between plume and MORB mantle sources.

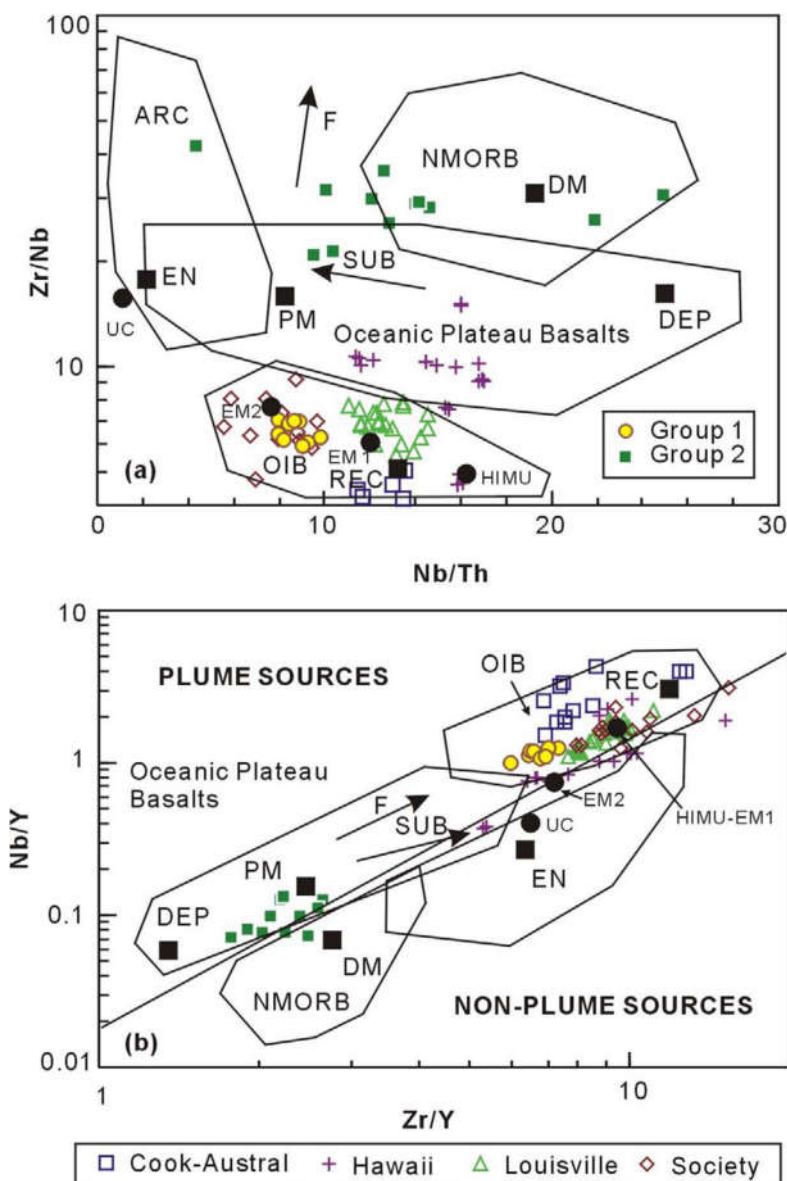


Fig. 9. Diagram showing mantle compositional components and fields for basalts from various tectonic settings (Condie, 2005). (a) Nb/Th versus Zr/Nb and (b) Zr/Y versus Nb/Y. Arrows indicate effects of batch melting (F) and subduction (SUB). Abbreviations: UC, upper continental crust; PM, primitive mantle; DM, shallow depleted mantle; HIMU, high Th/U mantle source; EM1 and EM2, enriched mantle sources; ARC, arc-related

basalts; NMORB, normal ocean ridge basalt; OIB, oceanic island basalt; DEP, deep depleted mantle; EN, enriched component; REC, recycled component. References: Weaver (1991), Condie (2003).

### 5.3. Seamounts in Junggar Ocean

The OIB-type pillow basalts that crop out in the Bayingou ophiolitic mélange of the North Tianshan occur in fault-bounded tectonic blocks within the mélange and are composed of massive basalts, gabbros, radiolarian cherts, pelagic limestones, basaltic breccias and tuffs. This ophiolitic mélange composition is similar to volcano-sedimentary sequences the accreted Paleogene ocean island sequences which are exposed in the Azuero Peninsula, west Panama (Buchs et al., 2011). Indeed, the association of basalt, breccia and limestone has been noted in many subduction–accretion complexes (e.g., Isozaki et al., 1990; Safonova and Santosh, 2014). Thus, we infer in conjunction with the geochemical signatures of the basalts, that the Bayingou ophiolitic mélange represents the remnants of a series of seamounts that are likely to have been oceanic islands or small plateaus. These fragments of seamounts are included in the imbricated thrust sheets and account for a relatively small volume of the mélange as the lowermost parts of the seamounts would have been subducted rather than

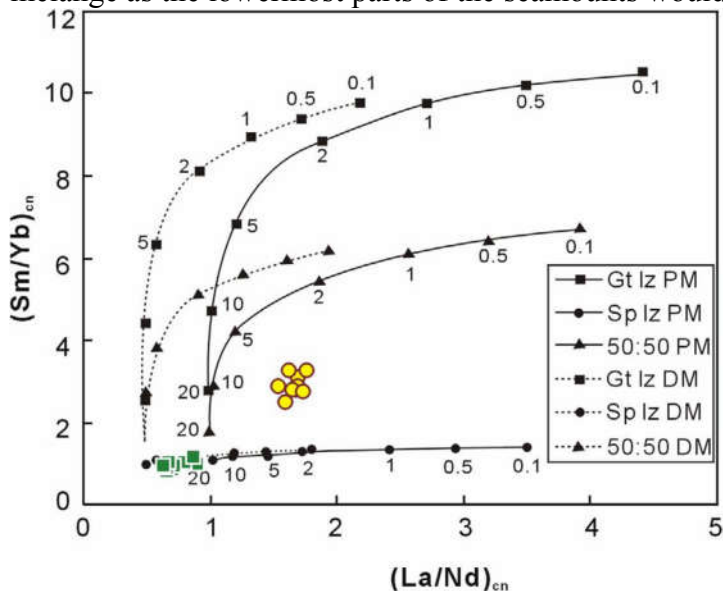


Fig. 10. Diagram showing the modelling results from pooled fractional melting calculations for various mantle source regions plotted on a  $(La/Nd)_{cn}$  versus  $(Sm/Yb)_{cn}$  diagram (after Kerr et al., 2015). Numbered ticks on the melting curves indicate percentage of partial melting. Gt, garnet; Sp, spinel; lz, lherzolite; PM, primitive mantle; DM, depleted mantle.

accreted during subduction–accretion processes (cf. Isozaki et al., 1990; Yang, 2016).

### 5.4. Geodynamic Implications for the Central Asian Orogenic Belt

The North Tianshan accretionary complex is one of the major accretionary complexes in the North Xinjiang region of western China and is located in the southeastern part of the Kazakhstan Orocline. The complex marks the final collision between the CTB in the south and the Junggar terrane in the north (Gao et al., 1997; Windley et al., 2007; Xiao et al., 2008; Zhu et al., 2009; An et al., 2013; Li et al., 2015). However, the timing of final subduction between CTB and Junggar terrane remains unclear. Xia et al. (2008) suggested that the complex formed in a rift setting in the Carboniferous due to the presence of so-called OIB-type volcanic rocks. However, Han et al. (2010) proposed that the collision occurred before the Late Carboniferous according to the presence of the Sikeshu ‘stitching pluton’ within the North Tianshan accretionary complex. Recently, Li et al. (2015) considered that the

subduction of the Junggar Ocean (a branch of the paleo-Asian Ocean) probably continued into the early Permian. Therefore, the accreted igneous rocks that it contains, such as the early Carboniferous Bayingou ophiolitic rocks of this study can shed new light on the evolution history of the North Tianshan accretionary complex.

This study, in conjunction with previous work (e.g., Wang et al., 2006; Han et al., 2010), supports the model that the Junggar Ocean, which was located between CTB and Junggar terrane, subducted southward beneath the CTB in the Late Devonian-Early Carboniferous. From this study it is clear that seamounts, comprising OIB-like pillow and massive basalts, dolerites and gabbros, developed on the ocean crust during its drift across a hotspot (Fig. 11a). As southward subduction proceeded, these upraised portions of oceanic crust were scraped-off and accreted in the wedge (Yang et al., 2015). Tectonic processes during accretion resulted in mixing of these fragments and the formation of an ophiolitic *mélange* in which the relicts of the seamounts are found as dismembered pieces (Fig. 11b). A recent review of OIB-bearing units in the CAO from the Late Neoproterozoic to Mesozoic by Safonova and Santosh (2014) suggested that the seamount-related magmatic activity was

**(a) Late Devonian-Early Carboniferous**

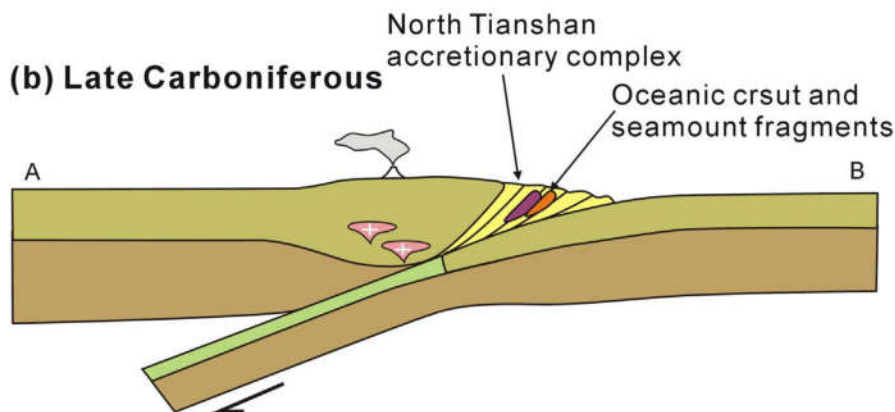
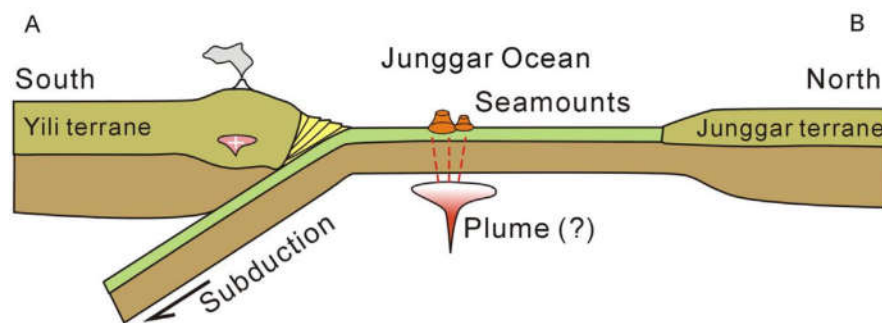


Fig. 11. Simplified geodynamic evolution of the Junggar Ocean in the Late Devonian-Late Carboniferous (after Han et al., 2010). Geodynamic reconstruction of the paleo-Asian Ocean based on Buslov et al. (2001). (a) Late Devonian- Early Carboniferous, the Junggar Ocean crust with seamounts were subducted southward beneath the Yili terrane. (b) In the Late Carboniferous, oceanic crust and seamounts were scraped-off and accreted in the accretionary complex resulting in the formation of the Bayingou ophiolitic *mélange*.

generally continuous during the development of the paleo-Asian Ocean (Yang et al., 2013, 2015). During the closure of the paleo-Asian Ocean, relict fragments of oceanic crust and seamounts were preserved as ‘ophiolites’ in the CAO accretionary complexes. In addition to the seamount fragments preserved in the ophiolitic *mélange*, the basement of the Tacheng block has recently been interpreted to represent a near-complete Early Paleozoic oceanic

plateau that was preserved in the accretionary complex of West Junggar (Zhang et al., 2017). It is widely accepted that there were multiple intra-oceanic subduction systems during the Paleozoic that closed the ocean basins which are now preserved in the CAO (e.g., Xiao et al., 2009). Therefore, the results of our study are consistent with the seamount accretion model to explain tectonic evolution of the CAO.

## 6. Conclusions

(1) The basaltic rocks in the Carboniferous Bayingou ophiolitic mélangé show two compositional groups: one ocean island basaltlike (Group 1) and the other mid-ocean ridge-like (Group 2), that can be distinguished on the basis of their pillow structure and immobile trace element contents.

(2) The ocean island basalt-like Group 1 are derived from a deeper garnet-bearing lherzolite source with lower degrees (2–3%) of melting. In contrast the more trace element-depleted Group 1 basalts are derived from a shallower spinel lherzolite mantle source with ~15% partial melting. Paradoxically, Group 2, despite having more depleted trace element signatures than Group 1, has a more enriched isotopic signature, implying that the source of Group 2 was depleted by melt extraction shortly before formation. Both groups lie on a mixing line between DMM and EM1.

(3) Both groups of basalts in the Bayingou ophiolitic mélangé represent the remnants of a series of seamounts, indicating that seamounts developed in the Junggar Ocean, as well as the paleo-Asian Ocean. Considering the spatial distribution of the Bayingou ophiolitic mélangé and the North Tianshan accretionary complex, we suggest that the seamount accretion occurred during the tectonic evolution of the North Tianshan.

## Acknowledgments

We sincerely thank Editor-in-Chief Professor Meifu Zhou and guest editor Professor Keda Cai and two anonymous reviewers for constructive reviews. This study was supported by the National Science Foundation of China (No. 41303027), the Young Star of Science and Technology Plan Projects in Shaanxi Province, China (No. 2016KJXX-71), and the Special Fund for Basic Scientific Research of Central Colleges, Chang'an University (Nos. 310827153506 and 310827153407).

## References

- Aldanmaz, E., Koprubasi, N., Gurer, Ö.F., Kaymakci, N., Gourgaud, A., 2006. Geochemical constraints on the Cenozoic, OIB-type alkali volcanic rocks of NW Turkey: implications for mantle sources and melting processes. *Lithos* 86, 50–76.
- Allen, M.B., Windley, B.F., Zhang, C., 1992. Palaeozoic collisional tectonics and magmatism of the Chinese Tien Shan, central Asia. *Tectonophysics* 220, 89–115.
- An, F., Zhu, Y.F., Wei, S.N., Lai, S.C., 2013. An early Devonian to early carboniferous volcanic arc in North Tianshan, NW China: Geochronological and geochemical evidence from volcanic rocks. *J. Asian Earth Sci.* 78, 100–113.
- Baksi, A.K., 2001. Search for a deep mantle component in mafic lavas using a Nb-Y-Zr plot. *Can. J. Earth Sci.* 38, 813–824.
- Buchs, D.M., Arculus, R.J., Baumgartner, P.O., Ulianov, A., 2011. Oceanic intraplate volcanoes exposed: Example from seamounts accreted in Panama. *Geology* 39, 335–338.
- Buchs, D.M., Hoernle, K., Hauff, F., Baumgartner, P.O., 2016. Evidence from accreted seamounts for a depleted component in the early Galapagos plume. *Geology* 44, 383–386.
- Buslov, M.M., Safonova, I.Yu., Watanabe, T., Obut, O., Fujiwara, Y., Iwata, K., Semakov, N.N., Sugai, Y., Smirnova, L.V., Kazansky, A.Yu., 2001. Evolution of the Paleo-Asian Ocean (Altai-Sayan region, Central Asia) and collision of possible Gondwanaderived terranes with the southern marginal part of the Siberian continent. *Geosci. J.* 5, 203–224.
- Carroll, A.R., Graham, S.A., Hendrix, M.S., Ying, D., Zhou, D., 1995. Late Paleozoic tectonic amalgamation of northwestern China: sedimentary record of the north Tarim, northwestern Turpan and southern Junggar basins. *Geol. Soc. Am. Bull.* 107, 571–594.
- Charvet, J., Shu, L.S., Laurent-Charvet, S., 2007. Paleozoic structural and geodynamic evolution of eastern Tianshan (NW China): welding of the Tarim and Junggar plates. *Episodes* 30, 162–186.
- Charvet, J., Shu, L.S., Laurent-Charvet, S., Wang, B., Faure, M., Cluzel, D., Chen, Y., De Jong, K., 2011. Palaeozoic tectonic evolution of the Tianshan Belt, NW China. *Sci. China, Ser. D Earth Sci.* 54, 166–184.
- Che, Z.C., Liu, H.F., Liu, L., 1994. Formation and Evolution of the Middle Tianshan Orogenic Belt. Geological Publishing House, Beijing pp. 1–135 (in Chinese).
- Chen, G.W., Deng, T., Xia, H., Liu, Q., 2012. Ocean island basalt associated with Bayingou ophiolite in West Tianshan Mountains: evidence from major and trace elements. *Acta Petrol. Mineral.* 31, 831–842.
- Condie, K.C., 2003. Incompatible element ratios in oceanic basalts and komatiites: tracking deep mantle sources and continental growth rates with time. *Geochim. Geophys. Geosyst.* 4 (1).
- Condie, K.C., 2005. High field strength element ratios in Archean basalts: a window to evolving sources of mantle plumes? *Lithos* 79, 491–504.
- Dong, Y.P., Zhou, D.W., Zhang, G.W., Zhao, X., Luo, J.H., Xu, J.G., 2006. Geology and geochemistry of the Gangou ophiolitic mélangé at the northern margin of the Middle Tianshan Belt. *Acta Petrol. Sin.* 22, 49–56 (in Chinese with English abstract).
- Dong, Y.P., Zhang, G.W., Zhou, D.W., Luo, J.H., Zhang, C.L., Xia, L.Q., Xu, X.Y., Li, X.M., 2007. Geology and geochemistry of the Bingdaban ophiolitic mélangé in the boundary fault zone on the northern Central Tianshan Belt, and its tectonic implications. *Sci. China (Series D)* 50, 7–21.
- Dong, Y.P., Zhang, G.W., Neubauer, F., Liu, X.M., Hauzenberger, C., Zhou, D.W., Li, W., 2011. Syn- and post-collisional granitoids in the Central Tianshan orogen: geochemistry, geochronology and implications for tectonic evolution. *Gondwana Res.* 20, 568–581.
- Ferrari, L., Petrone, C.M., Francalanci, L., 2001. Generation of oceanic-island basalt-type volcanism in the western Trans-Mexican volcanic belt by slab rollback, asthenosphere infiltration, and variable flux melting. *Geology* 29, 507–510.

- Fitton, J.G., Saunders, A.D., Norry, M.J., Hardarson, B.S., Taylor, R.N., 1997. Thermal and chemical structure of the Iceland plume. *Earth Planet. Sci. Lett.* 153, 197–208.
- Foulger, G.R., Natland, J.H., 2003. Is "hotspot" volcanism a consequence of plate tectonics? *Science* 300, 921–922.
- Gao, J., He, G.Q., Li, M.S., 1997. Paleozoic orogenic processes of Western Tianshan orogen. *Earth Science Journal of China University of Geosciences* 22, 27–32.
- Gao, J., Li, M.S., Xiao, X.C., Tang, Y.Q., He, G.Q., 1998. Paleozoic tectonic evolution of the Tianshan orogen, northwestern China. *Tectonophysics* 287, 213–231.
- Gao, J., Long, L.L., Klemd, R., Qian, Q., Liu, D.Y., Xiong, X.M., Su, W., Liu, W., Wang, Y.T., Yang, F.Q., 2009a. Tectonic evolution of the South Tianshan Orogen and adjacent regions, NW China: geochemical and age constraints of granitoid rocks. *Int. J. Earth Sci.* 98, 1221–1238.
- Gao, J., Qian, Q., Long, L.L., Zhang, X., Li, J.L., Su, W., 2009b. Accretionary orogenic process of Western Tianshan, China. *Geol. Bull. China* 28, 1804–1816.
- Godard, M., Bosch, D., Einaudi, F., 2006. A MORB source for low-Ti magmatism in the Semail ophiolite. *Chem. Geol.* 234, 58–78.
- Gou, L.L., Zhang, L.F., Tao, R.B., Du, J.X., 2012. A geochemical study of syn-subduction and post-collisional granitoids at Muzhaerte River in the Southwest Tianshan UHP belt, NW China. *Lithos* 136–139, 201–224.
- Han, B.F., He, G.Q., Wang, X.C., Guo, Z.J., 2011. Late Carboniferous collision between the Tarim and Kazakhstan-Yili terranes in the western segment of the South Tianshan Orogen, Central Asia, and implications for the Northern Xinjiang, western China. *Earth Sci. Rev.* 109, 74–93.
- Han, B.F., Guo, Z.J., Zhang, Z.C., Zhang, L., Chen, J.F., Song, B., 2010. Age, geochemistry, and tectonic implications of a late Paleozoic stitching pluton in the North Tianshan suture zone, western China. *Geol. Soc. Am. Bull.* 122, 627–640.
- Hauri, E.H., 1996. Major-element variability in the Hawaiian mantle plume. *Nature* 382, 415–419.
- Hemond, C., Hofmann, A.W., Vlastelic, I., Nauret, F., 2006. Origin of MORB enrichment and relative trace element compatibilities along the Mid-Atlantic Ridge between 10° and 24°N. *Geochim. Geophys. Geosyst.* 7. <http://dx.doi.org/10.1029/2006GC001317>
- Hirano, N., Takahashi, E., Yamamoto, J., Abe, N., Ingle, S.P., Kaneoka, I., Kimura, J., Hirata, T., Ishii, T., Ogawa, Y., Machida, S., Suyehiro, K., 2006. Volcanism in response to plate flexure. *Science* 313, 1426–1428.
- Hoernle, K., van den Bogaard, P., Werner, R., Lissinna, B., Hauff, F., Alvarado, G., Garbe-Schonberg, D., 2002. Missing history (16–71 Ma) of the Galapagos hotspot: Implications for the tectonic and biological evolution of the Americas. *Geology* 30, 795–798.
- Hofmann, A.W., 1997. Mantle geochemistry: the message from oceanic volcanism. *Nature* 385, 219–229.
- Huang, S.C., Regelous, M., Thordarson, T., Frey, F.A., 2005. Petrogenesis of lavas from Detroit seamount: geochemical differences between Emperor chain and Hawaiian volcanoes. *Geochim. Geophys. Geosyst.* 6, Q01L06. <http://dx.doi.org/10.1029/2004GC000756>.
- Isozaki, Y., Maruyama, S., Furuoka, F., 1990. Accreted oceanic materials in Japan. *Tectonophysics* 181, 179–205.
- Ivanov, V.A., Litasov, K.D., 2014. The deep water cycle and flood basalt volcanism. *Int. Geol. Rev.* 56, 1–14.
- Jensen, L.S., 1976. A new cation plot for classifying subalkalic volcanic rocks, vol. 66. Ontario Division Mines Miscellaneous.
- Jiang, T., Gao, J., Klemd, R., Qian, Q., Zhang, X., Xiong, X.M., Wang, X.S., Tan, Z., Chen, B.X., 2014. Paleozoic ophiolitic mélanges from the South Tianshan Orogen, NW China: geological, geochemical and geochronological implications for the geodynamic setting. *Tectonophysics* 612–613, 106–127.
- Kakar, M.I., Kerr, A.C., Mahmood, K., Collins, A.S., Khan, M., McDonald, I., 2014. Suprasubduction zone tectonic setting of the Muslim Bagh Ophiolite, northwestern Pakistan: insights from geochemistry and Sr-Nd isotopes. *Lithos* 202, 190–206.
- Kawahata, H., Nohara, M., Ishizuka, H., Hasebe, S., Chiba, H., 2001. Sr isotope geochemistry and hydrothermal alteration of the Oman ophiolite. *J. Geophys. Res.* 106, 11083–11100.
- Kerr, A.C., Tarney, J., Kempton, P.D., Pringle, M., Nivia, A., 2004. Mafic pegmatites intruding oceanic plateau gabbros and ultramafic cumulates from Bolívar, Colombia: evidence for a 'wet' mantle plume? *J. Petrol.* 45, 1877–1906.
- Kerr, A.C., Pearson, D.G., Nowell, G.M., 2009. Magma source evolution beneath the Caribbean oceanic plateau: new insights from elemental and Sr–Nd–Pb–HF isotopic studies of ODP Leg 165 Site 1001 basalts. In: James, K.H., Lorente, M.A., Pindell, J.L. (Eds.), *The Origin and Evolution of the Caribbean Plate*, vol. 328. Geological Society Special Publication, pp. 809–827.
- Kerr, A.C., Lavis, O., Kakar, M.I., McDonald, I., 2015. Petrogenesis and tectonomagmatic significance of Eocene mafic intrusions from the Neotethyan suture zone in the Muslim Bagh-Khanozai region, Pakistan. *J. Geol. Soc.* 173, 518–530.
- Khan, M., Kerr, A.C., Mahmood, K., 2007. Formation and tectonic evolution of the Cretaceous–Jurassic Muslim Bagh ophiolitic complex, Pakistan: implications for the composite tectonic setting of ophiolites. *J. Asian Earth Sci.* 31, 112–127.
- Kita, I., Yamamoto, M., Asakawa, Y., Nakagawa, M., Taguchi, S., Hasegawa, H., 2001. Contemporaneous ascent of within-plate type and island-arc type magmas in the Beppu-Shimabara graben system, Kyushu Island, Japan. *J. Volcanol. Geotherm. Res.* 111, 99–109.
- Kodaira, S., Takahashi, N., Nakanishi, A., Miura, S., Kaneda, Y., 2000. Subducted seamount imaged in the rupture zone of the 1946 Nankaido earthquake. *Science* 289, 104–106.
- Konopelko, D., Seltmann, R., Biske, G., Lepekhina, E., Sergeev, S., 2009. Possible source dichotomy of contemporaneous post-collisional barren I-type versus tin-bearing A-type granites, lying on opposite sides of the South Tien Shan suture. *Ore Geol. Rev.* 35, 206–216.
- Koppers, A.A.P., Watts, A.B., 2010. Intraplate seamounts as a window into deep Earth processes. *Oceanography* 23, 42–57.
- Lassiter, J.C., Blichert-Toft, J., Hauri, E.H., Barszczus, H.G., 2003. Isotope and trace element variations in lavas from Raiivavae and Rapa, Cook-Austral islands: constraints on the nature of HIMU- and EM-mantle and the origin of mid-plate volcanism in French Polynesia. *Chem. Geol.* 202, 115–138.
- Li, C., Xiao, W.J., Han, C.M., Zhou, K.F., Zhang, J.E., Zhang, Z.X., 2015. Late Devonian–early Permian accretionary orogenesis along the North Tianshan in the southern Central Asian Orogenic Belt. *Int. Geol. Rev.* 57, 1023–1050.
- Li, J.Y., He, G.Q., Xu, X., Li, H.Q., Sun, G.H., Yang, T.N., Gao, L.M., Zhu, Z.X., 2006a. Crustal tectonic framework of northern Xinjiang and adjacent regions and its formation. *Acta Geol. Sinica* 80, 149–168 (in Chinese with English abstract).
- Li, X.H., Li, Z.X., Wingate, M.T.D., Chung, S.L., Liu, Y., Lin, G.C., Li, W.X., 2006b. Geochemistry of the 755 Ma Mundine Well dyke swarm, northwestern Australia: part of a Neoproterozoic mantle superplume beneath Rodinia? *Precamb. Res.* 146, 1–15.
- Li, Y.J., Li, Z.C., Tong, L.L., Gao, Z.H., Tong, L.M., 2010. Revisit the constraints on the closure of the Tianshan ancient oceanic basin: new evidence from Yining block of the Carboniferous. *Acta Petrol. Sinica* 26, 2905–2912 (in Chinese with English abstract).
- Li, Y.J., Wu, L., Li, S.L., Li, G.Y., Shen, R., Li, Z., Wang, Z.P., Wang, Z.Y., 2017. Tectonic evolution of Yining Block: insights from Carboniferous volcanic rocks. *Acta Petrol. Sinica* 33, 1–15 (in Chinese with English abstract).
- Liu, D.D., Cheng, F., Guo, Z.J., Jolivet, M., Song, Y., 2015. Lahar facies of the Latest Paleozoic Arbasay Formation: geomorphological characters and paleoenvironment reconstruction of Northern Tianshan, NW China. *J. Asian Earth Sci.* 113, 282–292.
- Liu, S.W., Guo, Z.J., Zhang, Z.C., Li, Q.G., Zheng, H.F., 2004. Nature of Precambrian metamorphic blocks in eastern segment of the Central Tianshan: constraints from geochronology and Nd geochemistry. *Sci. China, Ser. D Earth Sci.* 47, 1085–1094.
- Long, L.L., Gao, J., Klemd, R., Beier, C., Qian, Q., Zhang, X., Wang, J.B., Jiang, T., 2011. Geochemical and geochronological studies of granitoid rocks from the Western Tianshan Orogen: implications for continental growth in the southwestern Central Asian Orogenic Belt. *Lithos* 126, 321–340.
- Lü, Z., Zhang, L.F., Du, J.X., Bucher, K., 2008. Coesite inclusions in garnet from eclogitic rocks in western Tianshan, northwest China: convincing proof of UHP metamorphism. *Am. Miner.* 93, 1845–1850.
- Ma, X.X., Shu, L.S., Meert, J.G., Li, J.Y., 2014. The Paleozoic evolution of central Tianshan: geochemical and geochronological evidence. *Gondwana Res.* 25, 797–819.
- Machida, S., Hirano, N., Sumino, H., Hirata, T., Yoneda, S., Kato, Y., 2015. Petit-spot geology reveals melts in upper-most asthenosphere dragged by lithosphere. *Earth Planet. Sci. Lett.* 426, 267–279.
- McDade, P., Blundy, J.D., Wood, B.J., 2003. Trace element partitioning on the Tinaquillo Lherzolite solidus at 1.5 GPa. *Phys. Earth Planet. Inter.* 139, 129–147.
- McKenzie, D., O'Nions, R.K., 1991. Partial melt distributions from inversion of rare earth element concentrations. *J. Petrol.* 32, 1021–1091.
- Morgan, W.J., 1971. Convection plumes in the lower mantle. *Nature* 230, 42–43.
- Mueller, W.U., Dostal, J., Stendal, H., 2002. Inferred Palaeoproterozoic arc rifting along a consuming plate margin: insights from the stratigraphy, volcanology and geochemistry of the Kangerluluk sequence, southeast Greenland. *Int. J. Earth Sci. (Geol. Rundsch.)* 91, 209–230.
- Nauret, F., Abouchami, W., Galer, S.J.G., Hofmann, A.W., Hemond, C., Chauvel, C., Dymont, J., 2006. Correlated trace element–Pb isotope enrichments in Indian MORB along 10°–20°S, Central Indian Ridge. *Earth Planet. Sci. Lett.* 245, 137–152.
- Niu, Y., Regelous, M., Wendt, J.J., Batiza, R., O'Hara, M.J., 2002. Geochemistry of near-EPR seamounts: importance of source vs. process and the origin of enriched mantle component. *Earth Planet. Sci. Lett.* 199, 327–345.
- Pearce, J.A., 1996. A user's guide to basalt discrimination diagrams. In: Wyman, D.A. (Ed.), *Trace Element Geochemistry of Volcanic Rocks: Applications for Massive Sulphide Exploration*, vol. 12. Geological Association of Canada, Short Course Notes, pp. 79–113.
- Pearce, J.A., Cann, J., 1973. Tectonic setting of basic volcanic rocks determined using trace element analyses. *Earth Planet. Sci. Lett.* 19, 290–300.
- Peng, R.M., Zhai, Y.S., Wang, Z.G., Han, X.F., 2005. Discovery of double-peaking potassium volcanic rocks in Langshan Group of the Tanyaokou hydrothermal-sedimentary deposit, Inner Mongolia, and its indicating significance. *Sci. China Ser. D-Earth Sci.* 48, 822–833.
- Polat, A., Hofmann, A.W., Rosing, M.T., 2002. Boninite-like volcanic rocks in the 3.7–3.8 Ga Isua greenstone belt, West Greenland: geochemical evidence for intra-oceanic subduction zone processes in the early Earth. *Chem. Geol.* 184, 231–254.
- Polat, A., Hofmann, A.W., 2003. Alteration and geochemical patterns in the 3.7–3.8 Ga Isua greenstone belt, West Greenland. *Precamb. Res.* 126, 197–218.
- Prendergast, E., Offer, R., 2012. Underplated seamount in the Narooma accretionary complex, NSW, Australia. *Lithos* 154, 224–234.
- Ranero, C.R., van Huene, R., 2000. Subduction erosion along the Middle America convergent margin. *Nature* 404, 748–752.
- Regelous, M., Hofmann, A.W., Abouchami, W., Galer, S.J.G., 2003. Geochemistry of lavas from the emperor seamounts, and the geochemical evolution of Hawaiian magmatism from 85 to 42 Ma. *J. Petrol.* 44, 113–140.
- Rodrigo-Gámiz, M., Martínez-Ruiz, F., Chiaradia, M., Jiménez-Espejo, F.J., Ariztegui, D., 2015. Radiogenic isotopes for deciphering tectrogenous input provenance in the western Mediterranean. *Chem. Geol.* 410, 237–250.
- Ruh, J.B., 2016. Submarine landslides caused by seamounts entering accretionary wedge systems. *Terra Nova* 28, 163–170.
- Safonova, I.Y., Santosh, M., 2014. Accretionary complexes in the Asia-Pacific region: tracing archives of ocean plate stratigraphy and tracking mantle plumes. *Gondwana Res.* 25, 126–158.
- Salteras, V.J.M., Longhi, J.E., Bizimis, M., 2002. Near mantle solidus trace element partitioning at pressures up to 3.4 GPa. *Geochim. Geophys. Geosyst.* 3, 1–23.
- Scott, C.R., Mueller, W.U., Pilote, P., 2002. Physical volcanology, stratigraphy, and litho-geochemistry of an Archean volcanic arc: evolution from plume-related volcanism to arc rifting of SE Abitibi Greenstone Belt, Val d'Or, Canada. *Precambrian Res.* 115, 223–260.
- Şengör, A.M.C., Natal'in, B.A., Burtman, U.S., 1993. Evolution of the Altaid tectonic collage and Paleozoic crustal growth in Eurasia. *Nature* 364, 299–306.
- Shu, L.S., Yu, J.H., Charvet, J., Laurent-Charvet, S., Sang, H.Q., Zhang, R.G., 2004. Geological, geochronological and geochemical features of granulites in the Eastern Tianshan, NW China. *J. Asian Earth Sci.* 24, 25–41.
- Simon, I., Jung, S., Romer, R.L., Garbe-Schönberg, D., Berndt, J., 2017. Geochemical and Nd–Sr–Pb isotope characteristics of synorogenic lower crust-derived granodiorites (Central Damara orogen, Namibia). *Lithos* 274–275, 397–411.

- Singh, S.C., Hananto, N., Mukti, M., Robinson, D.P., Das, S., Chauhan, A., Carton, H., Gratacos, B., Midnet, S., Djajadihardja, Y., Harjono, H., 2011. Aseismic zone and earthquake segmentation associated with a deep subducted seamount in Sumatra. *Nat. Geosci.* 4, 308–311.
- Staudigel, H., Koopers, A.P., Plank, T.A., Hanan, B.B., 2010. Seamounts in the subduction factory. *Oceanography* 23, 176–181.
- Staudigel, H., Clague, D.A., 2010. The geological history of deep-sea volcanoes: biosphere, hydrosphere, and lithosphere interactions. *Oceanography* 23, 58–71.
- Sun, S.S., McDonough, W.F., 1989. Chemical and isotopic systematics of oceanic basalts: implications for mantle composition and processes. In: Saunders, A.D., Norry, M.J. (Eds.), *Magmatism in the Ocean Basins*, vol. 42. Geological Society Special Publication, pp. 313–345.
- Tang, G.J., Wang, Q., Wyman, D.A., Sun, M., Li, Z.X., Zhao, Z.H., Sun, W.D., Jia, X.H., Jiang, Z.Q., 2010. Geochronology and geochemistry of Late Paleozoic magmatic rocks in the Lamasu-Dabate area, northwestern Tianshan (West China): evidence for a tectonic transition from arc to post-collisional setting. *Lithos* 119, 393–411.
- Tarduno, J.A., Duncan, R.A., Scholl, D.W., Cottrell, R.D., Steinberger, B., Thordason, T., Kerr, B.C., Neal, C.R., Frey, F.A., Torii, M., Carvallo, C., 2003. The Emperor Seamounts: southward motion of the Hawaiian hotspot plume in earth's mantle. *Science* 301, 1064–1069.
- Vanderkluysen, L., Mahoney, J.J., Koppers, A.A.P., Beier, C., Regelous, M., Gee, J.S., Lonsdale, P.F., 2014. Louisville Seamount Chain: petrogenetic processes and geochemical evolution of the mantle source. *Geochem. Geophys. Geosyst.* 15, 2380–2400.
- von Huene, R., 2008. When seamounts subduct. *Science* 321, 1165–1166.
- Wang, B., Faure, M., Cluzel, D., Shu, L.S., Charvet, J., Meffre, S., Ma, Q., 2006. Late Paleozoic tectonic evolution of the northern West Chinese Tianshan belt. *Geodin. Acta* 19, 237–247.
- Wang, B., Cluzel, D., Shu, L.S., Faure, M., Charvet, J., Chen, Y., Meffre, S., de Jong, K., 2009. Evolution of calc-alkaline to alkaline magmatism through Carboniferous convergence to Permian transcurrent tectonics, western Chinese Tianshan. *Int. J. Earth Sci.* 98, 1275–1298.
- Wang, B., Shu, L.S., Cluzel, D., Faure, M., Charvet, J., 2007a. Geochemical constraints on Carboniferous volcanic rocks of the Yili Block (Xinjiang, NW China): implication for the tectonic evolution of Western Tianshan. *J. Asian Earth Sci.* 29, 148–159.
- Wang, C., Liu, L., Che, Z.C., Luo, J.H., Zhang, J.Y., 2007b. Geochronology, petrogenesis and significance of Baleigong mafic rocks in Kokshal segment, Southwestern Tianshan Mountains. *Geol. Rev.* 53 (6), 743–754 (in Chinese with English abstract).
- Wang, M., Zhang, J.J., Zhang, B., Qi, G.W., 2015. An Early Paleozoic collisional event along the northern margin of the Central Tianshan Block: constraints from geochemistry and geochronology of granitic rocks. *J. Asian Earth Sci.* 113, 325–338.
- Watts, A.B., Koppers, A.A.P., Robinson, D.P., 2010. Seamount subduction and earthquakes. *Oceanography* 23, 166–173.
- Weaver, B.L., 1991. The origin of ocean island basalt end-member compositions: trace element and isotopic constraints. *Earth Planet. Sci. Lett.* 104, 381–397.
- Wessel, P., Sandwell, D.T., Kim, S.S., 2010. The global seamount census. *Oceanography* 23, 24–33.
- White, W.M., Duncan, R.A., 1996. Geochemistry and geochronology of the Society Islands: new evidence for deep mantle recycling. In: Basu, A., Hart, S.R. (Eds.), *Earth Processes, Reading the Isotopic Code*, AGU, Washington DC, pp. 183–206.
- Wilhem, C., Windley, B.F., Stampfli, G.M., 2012. The Altai of Central Asia: a tectonic and evolutionary innovative review. *Earth Sci. Rev.* 113, 303–341.
- Winchester, J.A., Floyd, P.A., 1977. Geochemical discrimination of different magma series and their differentiation products using immobile elements. *Chem. Geol.* 20, 325–343.
- Windley, B.F., Alexeiev, D., Xiao, W., Kröner, A., Badarch, G., 2007. Tectonic models for accretion of the Central Asian Orogenic Belt. *J. Geol. Soc. Lond.* 164, 31–47.
- Wu, J.Y., Liu, C.D., 1989. Geological features of Bayingou ophiolite complexes in North Tien Shan, Xinjiang. *Acta Petrol. Sinica* 2, 76–87 (in Chinese).
- Xia, L.Q., Xia, Z.C., Xu, X.Y., Li, M.X., Ma, Z.P., 2008. Relative contributions of crust and mantle to the generation of the Tianshan Carboniferous rift-related basic lavas, northwestern China. *J. Asian Earth Sci.* 31, 357–378.
- Xiao, W.J., Han, C.M., Yuan, C., Sun, M., Lin, S.F., Chen, H.L., Li, Z.L., Li, J.L., Sun, S., 2008. Middle Cambrian to Permian subduction-related accretionary orogenesis of Northern Xinjiang, NW China: implications for the tectonic evolution of central Asia. *J. Asian Earth Sci.* 32, 102–117.
- Xiao, W.J., Windley, B.F., Yuan, C., Sun, M., Han, C.M., Lin, S.F., Chen, H.L., Yan, Q.R., Liu, D.Y., Qin, K.Z., Li, J.L., Sun, S., 2009. Paleozoic multiple subduction-accretion processes of the southern Altai. *Am. J. Sci.* 309, 221–270.
- Xiao, W., Windley, B.F., Allen, M.B., Han, C., 2013. Paleozoic multiple accretionary and collisional tectonics of the Chinese Tianshan orogenic collage. *Gondwana Res.* 23, 1316–1341.
- Xiao, W.J., Santosh, M., 2014. The western Central Asian Orogenic Belt: a window to accretionary orogenesis and continental growth. *Gondwana Res.* 25, 1429–1444.
- Xiao, W.J., Windley, B.F., Sun, S., Li, J.L., Huang, B.C., Han, C.M., Yuan, C., Sun, M., Chen, H.L., 2015. A tale of amalgamation of three collage systems in the Permian-Middle Triassic in Central-East Asia: Oroclines, sutures, and terminal accretion. *Annu. Rev. Earth Planet. Sci.* 43, 16.1–16.31.
- Xiao, X.C., Tang, Y.Q., Feng, Y.M., Zhu, B.Q., Li, J.Y., Zhao, M., 1992. Tectonic Evolution of the Northern Xinjiang and its Adjacent Regions. Geology Publishing House, Beijing, pp. 1–169 (in Chinese with English abstract).
- Xie, W., Luo, Z.Y., Xu, Y.G., Chen, Y.B., Hong, L.B., Ma, L., Ma, Q., 2016. Petrogenesis and geochemistry of the Late Carboniferous rear-arc (or back-arc) pillow basaltic lava in the Bogda Mountains, Chinese North Tianshan. *Lithos* 244, 30–42.
- Xu, X.Y., Li, X.M., Ma, Z.P., Xia, L.Q., Xia, Z.C., Pen, G.X., 2006a. LA-ICPMS zircon U-Pb dating of gabbro from the Bayingou ophiolite in the northern Tianshan Mountains. *Acta Geol. Sin.* 80, 1168–1176 (in Chinese with English abstract).
- Xu, X.Y., Xia, L.Q., Ma, Z.P., Wang, Y.B., Xia, Z.C., Li, X.M., Wang, L.S., 2006b. SHRIMP zircon U-Pb geochronology of the plagiogranites from Bayingou ophiolite in the northern Tianshan Mountains and the petrogenesis of the ophiolite. *Acta Petrol. Sinica* 22, 83–94 (in Chinese with English abstract).
- Yang, G.X., 2016. Genesis of oceanic island basalt in ophiolitic mélange from core area of Central Asian Orogenic Belt. *Chin. Sci. Bull.* 61, 3684–3697 (in Chinese with English abstract).
- Yang, G.X., Li, Y.J., Gu, P.Y., Yang, B.K., Tong, L.L., Zhang, H.W., 2012a. Geochronological and geochemical study of the Darbut Ophiolitic Complex in the West Junggar (NW China): implications for petrogenesis and tectonic evolution. *Gondwana Res.* 21, 1037–1049.
- Yang, G.X., Li, Y.J., Santosh, M., Gu, P.Y., Yang, B.K., Zhang, B., Wang, H.B., Zhong, X., Tong, L.L., 2012b. A neoproterozoic seamount in the Paleozoic Ocean: evidence from zircon U-Pb geochronology and geochemistry of the Mayile ophiolitic mélange in West Junggar, NW China. *Lithos* 140–141, 53–65.
- Yang, G.X., Li, Y.J., Santosh, M., Yang, B.K., Zhang, B., Tong, L.L., 2013. Geochronology and geochemistry of basalts from the Karamay ophiolitic mélange in West Junggar (NW China): implications for Devonian-Carboniferous intra-oceanic accretionary tectonics of the southern Altai. *Geol. Soc. Am. Bull.* 125, 401–419.
- Yang, G.X., Li, Y.J., Xiao, W.J., Tong, L.L., 2015. OIB-type rocks within West Junggar ophiolitic mélanges: Evidence for the accretion of seamounts. *Earth Sci. Rev.* 150, 477–496.
- Zhang, J.E., Xiao, W.J., Luo, J., Chen, Y.C., Windley, B.F., Song, D.F., Han, C.M., Safonova, I., 2017. Collision of the Tacheng block with the Mayile-Barleik-Tanghale accretionary complex in Western Junggar, NW China: implication for Early-Middle Paleozoic architecture of the western Altai. *J. Asian Earth Sci.* <http://dx.doi.org/10.1016/j.jseas.2017.03.023>.
- Zheng, J.P., Griffin, W.L., O'Reilly, S.Y., Zhang, M., Liou, J.G., Pearson, N., 2006. Granulite xenoliths and their zircons, Tuoyun, NW China: insights into southwestern Tianshan lower crust. *Precamb. Res.* 145, 159–181.
- Zhong, L.L., Wang, B., Shu, L.S., Liu, H.S., Mu, L.X., Ma, Y.Z., Zhai, Y.Z., 2015. Structural overprints of early Paleozoic arc-related intrusive rocks in the Chinese Central Tianshan: implications for Paleozoic accretionary tectonics in SW Central Asian Orogenic Belts. *J. Asian Earth Sci.* 113, 194–217.
- Zhu, Y.F., Guo, X., Song, B., Zhang, L.F., Gu, L.B., 2009. Petrology, Sr–Nd–Hf isotopic geochemistry and zircon chronology of the Late Paleozoic volcanic rocks in the southwestern Tianshan Mountains, Xinjiang, NW China. *J. Geol. Soc. Lond.* 166, 1085–1099.
- Zhu, Y.F., Zhang, L.F., Gu, L.B., Guo, X., Zhou, J., 2005. The zircon SHRIMP chronology and trace element geochemistry of the Carboniferous volcanic rocks in western Tianshan Mountains. *Chin. Sci. Bull.* 50, 2201–2212.
- Zindler, A., Hart, S., 1986. Chemical geodynamics. *Annu. Rev. Earth Planet. Sci.* 14, 493–571.